Geophysical Journal International

Geophys. J. Int. (2025) **242,** 1–19
Advance Access publication 2025 June 26
Applied and marine geophysics

https://doi.org/10.1093/gji/ggaf236

Stochastic inversion of transient electromagnetic data to derive aquifer geometry and associated uncertainties

Lukas Aigner [1], Hadrien Michel [2], Thomas Hermans [3] and Adrián Flores Orozco [1]

[1] *Research Unit Geophysics, Department of Geodesy and Geoinformation, TU Wien,* A-1040 *Vienna, Austria. E-mail: lukas.aigner@geo.tuwien.ac.at*
[2] *Urban and Environmental Engineering Department, Faculty of Applied Sciences, University of Liege,* B-4000 *Liege, Belgium*
[3] *Department of Geology, Ghent University, Krijgslaan* 281-*S*8, B-9000 Gent, *Belgium*

Accepted 2025 June 17. Received 2025 May 20; in original form 2024 October 25

SUMMARY

Understanding processes in the Critical Zone requires reliable information about the vadose-zone aquifer, its geometry, and spatial variability. Commonly, such information is obtained from boreholes, yet large areas might render their application prohibitively expensive. Additionally, limited geological *a-priori* information might bias the interpretation due to lateral geological changes smaller than the borehole sampling scale. The transient electromagnetic method (TEM) has emerged in the last decades as a well-suited method to efficiently investigate the subsurface, as required for many hydrogeological applications. The interpretation of TEM measurements relies mainly on deterministic inversions, offering only a limited insight on the uncertainty of the subsurface model. Uncertainty quantification, however, is essential for integrating TEM results into hydrogeological models. Hence, we propose a combined approach using both deterministic and stochastic inversion of TEM soundings to investigate the uncertainty of shallow (< 40 m) aquifers. Current stochastic approaches for TEM data rely on Markov chain Monte Carlo algorithms, which have to be run from scratch for each individual sounding. Alternatively, machine learning approaches, such as Bayesian Evidential Learning (BEL), can be much faster because they do not require retraining for every new data set. Hence, we investigate, in particular, the application of a single, common prior model space instead of multiple, individual prior model spaces to directly estimate the uncertainty of multiple TEM soundings. To this end, we combine forward modelling routines with the stochastic inversion approach BEL1D and assess our approach using both field data and numerical experiments.

Key words: Electrical properties; Controlled source electromagnetics (CSEM); Machine learning; Statistical methods; Hydrogeophysics.

1 INTRODUCTION

Critical zone science is an emerging interdisciplinary field that requires reliable information on the geometry of vadose-zone aquifer and aquitard systems (e.g. Singha & Navarre-Sitchler 2022; Hermans *et al.* 2023). This is essential, for instance, to quantify surface-groundwater interactions (e.g. Winter 2000; Fleckenstein *et al.* 2010; Ntona *et al.* 2022), to investigate the fate and transport of contaminants in the groundwater (e.g. Atekwana & Atekwana 2010; Cassiani *et al.* 2014; Flores Orozco *et al.* 2021) and to characterize sea-water intrusion in coastal areas (e.g. Goldman *et al.* 1991; Guérin *et al.* 2001; Paepen *et al.* 2020; Cong-Thi *et al.* 2021; Deleersnyder *et al.* 2023, among others). Critical zone investigations commonly rely on a limited number of boreholes where groundwater levels are measured together with grain size analysis. Subsequently, continuous and areal information is inferred by interpolation of borehole data, which might bias the interpretation in particular for heterogeneous sites (e.g. Schulze-Makuch *et al.* 1999). Geophysical methods allow to map the subsurface in a quasi-continuous and non-invasive way (e.g. Binley *et al.* 2015). Due to the relationship between electrical resistivity and textural properties of geological materials, the electrical resistivity tomography (ERT) is commonly applied to delineate the geometry of aquifers and hydraulic barriers (e.g. Binley *et al.* 2015). Yet, an extensive survey area or a large depth of investigation require long survey layouts, involving the logistics of moving heavy cables to map an area of interest and thus, leading to relatively long acquisition times. Alternatively, the transient electromagnetic (TEM) method has emerged as a suitable technique for hydrogeological investigations (e.g. Fitterman & Stewart 1986; Meju *et al.* 1999; Auken *et al.* 2003; Danielsen *et al.* 2003; Christiansen *et al.* 2006). Recent advances in instrumentation for waterborne (e.g. Lane *et al.* 2020; Yogeshwar *et al.* 2020; Bücker *et al.* 2021 and Aigner *et al.* 2021) and ground-based applications (e.g. Auken *et al.* 2018 and Street *et al.* 2018) have demonstrated

the potential of the TEM method to collect extensive 3-D data sets to obtain the subsurface electrical resistivity in quasi real-time.

Modelling and inversion techniques can use tens to thousands of soundings to resolve for 2-D and 3-D models of the subsurface (e.g. Yogeshwar *et al.* 2020; Grombacher *et al.* 2022; Kang *et al.* 2022). Commonly, the inversion of TEM soundings relies on deterministic inversion algorithms (e.g. Auken *et al.* 2015; Heagy *et al.* 2017), which require a spatial regularization in the model space to enhance the consistency between the inverted model parameters and reduce the effect of data-error in the inverted model (e.g. Tikhonov & Arsenin 1977; Tarantola 2005). Deterministic inversions use either models with a small and pre-defined number of layers where both the electrical resistivity and the layer thickness are variable, or models consisting of many fixed-thickness layers with a smoothness constraint (e.g. Minsley 2011). Deterministic inversions are affected by the ill-posedness of the problem, leading to a large number of models being able to explain the data. Moreover, deterministic inversion schemes allow only for a limited quantification of uncertainty based on the propagation of the data error assuming a Gaussian distribution of the data error (e.g. Aster *et al.* 2005, 2018), for instance obtained from the linearized Jacobian matrix (e.g. Christiansen & Auken 2012).

Stochastic approaches offer the advantage of exploring the full prior distribution of the model parameters, removing any hypothesis on the linearity of the model and the noise distribution (e.g. Tarantola 2005). Some of the first applications of stochastic methods to electromagnetic data is attributed to Minsley (2011) and Trainor-Guitton & Hoversten (2011). Minsley (2011) used a trans-dimensional Markov chain Monte Carlo (McMC) algorithm to retrieve the full posterior distribution of subsurface model parameters from frequency-domain EM data using ground-based and airborne EM systems. The same algorithm was successfully applied by Ball *et al.* (2020) to quantify a freshwater-brine interface, and Minsley *et al.* (2021) expanded the algorithm to include time-domain EM measurements. This parsimonious McMC algorithm has the advantage of determining the unknown number of layers with changing electrical properties in the subsurface. More recently, Blatter *et al.* (2018) and Ray *et al.* (2023) have applied an McMC algorithm to TEM measurements obtained in Antarctica and Australia imaging hydrogeological structures and incorporating airborne system parameters. However, McMC algorithms require 100 000s iterative forward modelling runs to converge towards a static posterior distribution making them computational expensive. The computational timescales with the number of soundings, as the forward modelling must be run for every single sounding position to estimate the posterior distribution for each sounding.

Recently, Bayesian evidential learning (BEL) has emerged as a suitable alternative to approximate the posterior uncertainty and has been applied successfully to hydrogeological applications (e.g. Scheidt *et al.* 2015, 2018). BEL was successfully applied to problems covering flow-based inverse modelling (Scheidt *et al.* 2015), heat-storage capacity of an aquifer monitored with electrical resistivity tomography (Hermans *et al.* 2018) and experimental design comparing well and geophysical data for temperature monitoring (Thibaut *et al.* 2022). Within the context of geophysical inversion, BEL establishes a direct relationship between model and data space, leading to a significant reduction of computational time, with the added benefit that forward modelling runs can be reused to estimate the posterior distribution of many different data sets if the exact same system configuration is used (e.g. Michel *et al.* 2020). The BEL framework was expanded to allow the direct estimation of 1-D model parameter uncertainty from surface nuclear magnetic resonance (SNMR) sounding establishing Bayesian Evidential Learning 1-D (BEL1D) imaging (Michel *et al.* 2020). The accuracy of BEL1D to estimate the uncertainty was enhanced by applying iterative prior resampling (IPR) and rejection sampling (RS; Michel *et al.* 2023). IPR and RS were developed to reduce the inefficiency associated with large prior model spaces that might result in an overestimation of uncertainty. The authors benchmarked their algorithm against an McMC approach based on a Metropolis Hastings algorithm with multiple chains (e.g. Vrugt & Ter Braak 2011, and references therein) showing that BEL1D together with IPR and RS yields an approximation of the posterior distribution close to the one obtained by McMC, yet significantly (95 per cent) reducing the computational time (see Michel *et al.* 2023). Recently, Ahmed *et al.* (2024) demonstrated that a similar reduction in posterior uncertainty, comparable to that from IPR and RS, can be obtained using a simple and efficient, misfit-based, threshold-rejection (TR) approach, thereby eliminating the need for IPR.

We investigate the geometry of a shallow aquifer based on single-loop TEM soundings. The objective of this study is to quantify the uncertainty of the subsurface model parameters (i.e. layer thickness and resistivity). Our approach utilizes a combined approach based on initial deterministic inversion to formulate an informed prior model space for BEL1D. This combined approach allows for a similar uncertainty reduction, as previously reported by Michel *et al.* (2023) using IPR and RS, while allowing to re-use the informed prior model for other TEM soundings. We investigate, in particular, whether stochastic inversion of each sounding independently retrieves similar uncertainties as the inversion of all soundings using the same common prior model space. We expect that the main benefit of the common prior space approach is a reduction of the computational time compared to individual prior model spaces for each sounding position. We note that a prior definition based on the deterministic solution together with the TR approach, based on relative root-mean-square errors as employed here, yields a pragmatic estimation of the posterior uncertainty, but not the true uncertainty as given by a rigorous Bayesian posterior (see Scales & Snieder 1997).

Our work is organized as follows. We start by briefly describing the TEM method and the associated modelling approach, continue with the BEL1D methodology and describe the field data as well as the numerical experiments. Then we demonstrate that the stochastic inversion yields similar results as the deterministic inversion for two independent soundings and evaluate our results by comparing to the lithology from two boreholes. This is followed by field measurements along a profile to demonstrate that a common prior model space can estimate similar uncertainties as individual prior model spaces for each sounding position for a laterally homogeneous subsurface. We then evaluate this common prior approach in a laterally heterogenous numerical experiments. We conclude with a discussion of the added value of the common prior approach and the future perspectives associated to this study.

2 MATERIAL AND METHODS

2.1 Transient electromagnetic method—basics, instrumentation and processing

The TEM method can be applied in different configurations (e.g. Nabighian *et al.* 1991), yet in this work we focus on the single-loop

configuration, aiming at simplifying field procedures, for instances in comparison with separated transmitter and receiver loop antennas. A direct current is circulated in the horizontal square loop antenna and interrupted causing the primary magnetic field to decay over time. This primary field induces eddy currents into the ground which diffuse downward and laterally into the subsurface over time generating a secondary magnetic field (e.g. Nabighian 1979). The temporal change of the secondary magnetic field can be measured as a voltage-decay induced into a receiver loop antenna at the surface. The shape of the resulting decay curve depends on the electrical resistivity (ρ) of the subsurface. High values of ρ reduce the signal strength of the secondary magnetic field, while low values of ρ enhance the signal strength. The voltage decay is commonly measured in logarithmically distributed time windows which results in a few tens of individual voltage readings ranging from a couple of microseconds up to hundreds of milliseconds.

Field data measurements were obtained with the TEM-FAST 48 system manufactured by AEMR (Applied Electromagnetic Research, Utrecht, the Netherlands). The TEM-FAST system allows injecting transmitter currents of 1 A or 4 A and the voltage decay can be measured in up to 48 logarithmically distributed time windows ranging from 4 μs to 16 ms. The transmitter current has a trapezoidal shape, where the front ramp is constant at 30 μs and the width of the current pulse ranges between 0.23 and 67.50 ms.

2.2 Forward modelling, deterministic inversion and distance-based global sensitivity analysis

We use the 1-D TEM forward modeller proposed by Aigner *et al.* (2024), which is based on the open-source library empypmod by Werthmüller (2017). These routines use the vertical transversal isotropic approach which requires simple 1-D models consisting of the layer thickness (thk) and the corresponding electrical resistivity (ρ). Additionally, the forward modeller employs the quasi-static approximation and models the single-loop configuration with a vertical magnetic dipole in the centre of the transmitter loop. For the deterministic inversion, we use routines available in pyGIMLi (Rücker *et al.* 2017) that were connected to the forward modelling (for details see Aigner *et al.* 2024). In particular, we use a Marquardt-type inversion approach and formulate three different stopping criteria: (1) maximum of 25 iterations, (2) reaching an error-weighted root-mean-square error of the data misfit < 1, (3) difference of consecutive iterations <2 per cent. The layer thickness is allowed to vary in a range of 1 to 100 m, while the electrical resistivity is allowed to vary in a range of 1 to 1000 Ωm. We perform a distance-based global sensitivity analysis (DGSA, e.g. Fenwick *et al.* 2014; Perzan *et al.* 2021) as described by Aigner *et al.* (2024) to derive the global sensitivity of the model parameters (thk and ρ) directly from the prior model and data space obtained in the initial step of BEL1D (see Hermans *et al.* 2018). Such global sensitivities evaluate the influence that each model parameter has on the model response.

2.3 Bayesian evidential learning—BEL1D

We estimate the uncertainty associated to subsurface electrical parameters with the Bayesian evidential learning 1D (BEL1D) imaging framework that is described in depth by Michel *et al.* (2020). BEL1D obtains an approximation of the posterior distribution for the model parameters using six main steps, namely: (1) forward modelling of TEM responses from a prior model space for a given range of model parameters, commonly in a uniform distribution, (2) dimensionality reduction of the data and model space using principal component analysis (PCA, e.g. Krzanowski 2000), (3) establishing statistical relationship between the reduced data and model space using canonical correlation analysis (CCA), (4) application of kernel density estimation (KDE) to determine an approximation of the posterior distribution in the CCA model space that is constrained to the field data, (5) sampling of the obtained posterior distribution with the inverse transform method and (6) back-transformation of the samples into the original data and model space by applying the inverse CCA transformation followed by the corresponding PCA back transformations. Further details on the general idea behind Bayesian evidential learning (BEL) can be found in Scheidt *et al.* (2018), while the system of equations including the noise propagation is available in Hermans *et al.* (2016). The main difference to our work is the usage of a KDE to approximate the joint probability density function in the CCA space (instead of Gaussian linear regression), which has the advantage of working also when the relationship between reduced data and model space is not perfectly linear (as detailed in Michel *et al.* 2020). In our analysis, we provide only a visual quantification of the information gain (e.g. Lindley 1956), in contrast with previous studies that offer a rigorous, mathematical quantification of the information gain (e.g. Ray *et al.* 2023; Strutz & Curtis 2023).

We generate a prior model space based upon an initial deterministic inversion of the TEM data using an n-layer model with variable layer thickness, where n is the number of layers and n is chosen based upon prior knowledge of the site. We use the deterministic inversion result to determine a prior range for each model parameter (i.e. thickness and ρ) with a minimum and maximum that is equal to $\pm$ 1/4 of the model parameter value for each individual sounding, resulting in a prior mean that is equal to each deterministic inversion result. In the case of TEM soundings along a profile, we also investigate the use of a common prior space that is formulated based on the deterministic inversion results of all soundings along the profile. For the common prior model space, we use a minimum and maximum prior boundary based on subtracting 1/4 of the minimum and adding 1/4 to the maximum of all deterministic inversion result parameters (i.e. thickness and ρ). We forward calculate the prior data space from 30 000 models uniformly distributed in the prior model space to achieve a sufficient sampling of the parameter space. In initial tests, we observed that the rather simple TEM decay curve can be sufficiently (i.e. larger than 95 per cent explained variance) described by only 3 to 5 dimensions, while the model space typically requires between 5 and10 PCA dimensions due to the larger complexity. The subsequent back-transformation after CCA and KDE requires that the PCA-reduced data space must have an equal or larger amount of dimensions than the PCA-reduced model space. Yet, the TEM data space requires a PCA dimensionality reduction using fewer than 10 dimensions to facilitate a correct establishment of the statistical relationship between reduced data and model with CCA. In our numerical data experiments, we use 5 PCA dimensions for the reduction of both the model and data space, while we use 10 PCA dimensions in the case of field data resulting in an explained variance larger than 95 perc ent in all the investigated data sets. The larger number of PCA dimensions for the field data is related to a doubling of the layer number in the field case. For the posterior model sampling, we use 15 000

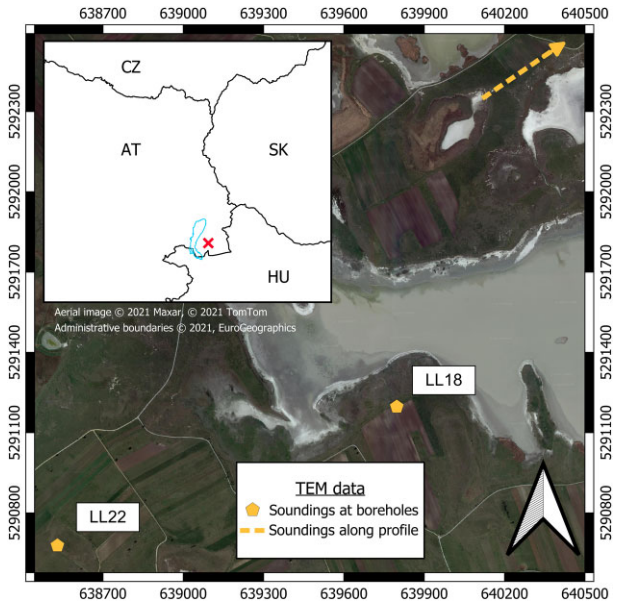

Figure 1. Overview of the field data measured at the soda lakes test site and the position of the test site within Austria (AT) and its neighbouring countries (HU—Hungary, SK—Slovakia, CZ—Czech Republic).

models per sounding to ensure a dense sampling of the posterior distribution.

Compared to previous work by Michel *et al.* (2023), we do not apply IPR and RS because initial tests have shown that a simple threshold rejection (TR) based on the data misfit between measured data and posterior data samples leads to similar results obtained with IPR and RS. All BEL1D calculations were done with the adapted pyBEL1D routines published by Michel (2022). Throughout our work, we compute the relative root-mean-square error (rRMSE, see appendix of Aigner *et al.* 2024) using log-scaled differences between the measured data and model responses (see Ahmed *et al.* 2024) and set the rejection threshold to 3 per cent. In principle, TR is not aligned with the original idea of BEL or stochastic theory in general, because the application of a hard threshold (i.e. no probability rule) does not lead to convergence towards the 'true' posterior distribution. Yet, TR offers an efficient method to approximate the posterior distribution by removing unrealistic models from the posterior model space and efficiently reducing the estimated uncertainty (see Ahmed *et al.* 2024). In addition, TR alleviates the need for additional forward model runs as in IPR, which opens the possibility to use a common prior to invert multiple soundings drastically reducing computational time.

2.4 Case studies: transient electromagnetic field data, lithological information from boreholes and numerical experiments

Field measurements were done in Burgenland, Austria (47°46'12.2"N 16°52'12.3"E) within the soda lakes of the 'Nationalpark Neusiedlersee—Seewinkel'. We collected TEM data at two ca. 10 m deep historical boreholes (see page 30 in Hermann 2023) available in the vicinity of the profile (see Fig. 1) to evaluate the accuracy of the resistivity model obtained with the deterministic and stochastic inversion algorithms. The borehole lithology also allows a direct interpretation of the electrical resistivity in terms of geological materials. We also collected data along a single profile at 36 sounding positions to determine the depth and the thickness of a confined aquifer. The site consists of two sandy gravel aquifers confined between silt rich layers.

The TEM data collected at the boreholes were measured with a 6.25 m loop, a 12.5 m loop and a 25.0 m loop to investigate the different sensitivities associated with a change of the transmitter waveform (i.e. turn-off ramp) due to the increased self-inductance of the larger loops. A comprehensive overview of the measurement settings can be found in Table 1. We use a homogeneous five-layer initial model for the deterministic inversion of all field data and centre the prior model space for BEL1D on the deterministic inversion result.

TEM field data were collected along a 2-D profile using a 12.5 m square loop during May of 2022 in dry surface conditions. We used 4 A of transmitter current and collected voltage readings by stacking the data 8320 times in 28 windows ranging from 4 to 512 μs. For all field measurements, we use the error estimation by the TEM-FAST device but adjust relative data errors below a 3 per cent threshold to 3 per cent, as experiments have shown that the device underestimates the actual data error.

Our numerical data experiments aim at comparing results obtained from individual prior models for every sounding and a common prior model space for all soundings. The numerical data were generated for five soundings positions forming a profile that extends over 250 m with equal distances between soundings. We simulate the data using a 12.5 m single loop configuration with an injected current of 4.0 A and we contaminate the data with a relative error of 3 per cent and use the same error values to define the error model in the inversion. The numerical models represent a confined aquifer system with varying depth and thickness of the aquifer. Low resistivity values ($< 30\ \Omega$m) of the top and bottom layers represent a higher fraction of fine grained materials which act as a hydraulic barrier, while the high resistivity in the second layer (200 Ωm) represents the aquifer in sandy gravels (see Table 2). We use a three-layer initial model where each layer has the same resistivity (50 Ωm) for the deterministic inversion of the numerical data.

Table 1. Overview of the TEM-FAST 48 measuring settings for TEM data collected at the borehole positions including: the loop size (side-length of the square), the injected current, the turn-off ramp, the number of stacks, the number of gates for observing the transient decay and the maximum time (t_{max}) at which the last gate is located. The first gate is at 4 μs for all soundings.

		Borehole: LL18				Borehole: LL22		
Loop (m)	Current (A)	Ramp (μs)	Stacks ()	Gates ()	t_{max} (ms)	Stacks ()	Gates ()	t_{max} (ms)
6.25	4.3	0.5	33280	24	0.24	66560	20	0.12
12.5	4.3	0.95	8320	32	0.96	13312	28	0.48
25.0	4.2	1.5	8320	36	1.90	8320	36	1.90

Table 2. Overview of the model parameters for generating numerical data including the sounding name, the pseudo distance, the layer thickness thk and the electrical resistivity ρ.

		Layer 1, soil, silts		Layer 2, aquifer, sandy gravels		Layer 3, aquiclude, silts	
Name	Distance (m)	thk (m)	ρ (Ω m)	thk (m)	ρ (Ω m)	thk (m)	ρ (Ω m)
T01	50	4	30	18	200	∞	15
T02	100	9	30	18	200	∞	15
T03	150	14	30	23	200	∞	15
T04	200	11.5	30	15	200	∞	15
T05	250	6.5	30	15	200	∞	15

3 RESULTS

3.1 Proof of concept: evaluation of the stochastic inversion using deterministic results and borehole data

The main goal of this section is to demonstrate that the stochastic inversion of TEM data collected at two boreholes can retrieve changes in electrical resistivity that correspond to the soil composition as observed in the borehole lithology. The TEM inversion results and lithology for boreholes LL18 and LL22 is presented in Fig. 2 for two different loop sizes. In general, we observe a three-layer model which corresponds to a confined aquifer. The stochastic inversion results (Figs 2b and f) show similar three-layer models as the deterministic results (Figs 2a and e) and the resistivity contrasts are in agreement with the borehole lithology. The first layer is characterized by low electrical resistivity (< 10 Ωm) corresponding to the organic soils and clayey silts. The second layer is characterized by high electrical resistivity (ca. 100 Ωm) corresponding to the aquifer in sands and gravels. The third layer is characterized by low electrical resistivity (< 20 Ωm) corresponding to clayey silts acting as the confining layer below the aquifer. At borehole LL18 we observe an additional fourth layer that shows an increase in electrical resistivity (ca. 30 Ωm) which might correspond to a second aquifer. This fourth layer cannot be seen in the borehole due to the limited depth of ca. 11 m and therefore we will not discuss the fourth layer further.

Fig. 2(b) shows the uncertainty for TEM data collected at borehole LL18, while Figs 2(c) and (d) show the global sensitivity from the DGSA. The low resistive first layer obtained from both the 6.25 and 12.5 m loops correctly resolves the clayey silt layer. The uncertainty of electrical resistivity is lower for the 12.5 m loop than for the 6.25 m loop, in particular for the aquifer (layer two, between 2.5 and 7.5 m). The low uncertainty of electrical resistivity for the 12.5 m loop corresponds well with the high global sensitivity for the resistivity of the first three layers. The uncertainty of the layer thickness increases with increased depth, as expected considering that the deeper layers are significantly less sensitive to the measured data. The 6.25 m loop likely overestimates the resistivity in case of layers with high resistivity (i.e. > 30 Ωm).

Fig. 2(f) shows the uncertainty for TEM data collected at borehole LL18, while Figs 2(g) and (h) show the global sensitivity from the DGSA. The 6.25 m loop correctly estimates the depth to the aquifer with a low uncertainty (ca. 1.2 m $\pm$ 0.1 m) and the thickness of the first layer is also the most sensitive parameter of the inversion as resolved by the DGSA (see Fig. 2g). Similar to the TEM results at borehole LL18, we observe that an increase in resistivity, also increases the uncertainty of the actual value resolved, which corresponds also to a lower global sensitivity. The depth to the bottom of the aquifer is slightly overestimated by both loop sizes as we observe a depth of 9.0 m to the confining layer indicated by lower resistivity (20 Ωm) compared to a lithological change (from gravels to silts) at already 7.8 m depth. The stochastic inversion resolves an uncertainty of $\pm$ 2.0 m for the depth to this interface. Thus, the interpretation of the resistive layers is improved as we can now estimate the accuracy of the aquifer geometry from the TEM soundings, which is not possible with the deterministic inversion or the DGSA alone.

Fig. 3 visually shows the information gain at borehole LL18 for the 6.25 and the 12.5 m loops by comparing the prior data and model spaces to the posterior (after TR) data and model spaces. We can observe that the model response of the mean model fits the observed data well (see Figs 3a and c). In general, Fig. 3 shows that the uncertainty is lower closer to the surface and for layers with a lower electrical resistivity. This increase of the uncertainty with depth is also reflected in an increased range of the late time (ca. 1×10^{-4} s) posterior data distributions. This result validates the chosen prior range around the deterministic inversion, because extreme models are rejected, while more conservative models are kept. An increase of the prior range, would only lead to an increased number of rejected models. Hence, our chosen prior space leads to an adequate approximate of the uncertainty. All of these observations are also valid for the inversion of the sounding at borehole LL22 as seen in Fig. A2 in the Appendix.

3.2 Estimation of the aquifer geometry from TEM field data at the soda lakes

To demonstrate the applicability of BEL1D on TEM data and investigate stochastic inversion results from individual prior spaces and a single common prior space, we present field data results for 36 soundings collected along a profile with a length of 460 m. The deterministic and stochastic inversion results (Fig. 4) reveal, in general, a three layer model consisting of: (1) a first layer with a thickness of ca. 10 m and a resistivity ranging between 15 and 40 Ωm corresponding to sandy gravels associated to the shallow aquifer, (2) a conductive ($\rho < 15$ Ωm) second layer with a thickness of ca. 13 m corresponding to a confining layer of clayey silts at a depth of ca. 10 m and (3) a third layer with intermediate resistivity values (ca. 25 Ωm) corresponding to sandy material constituting a second aquifer at a depth of ca. 25 m. The first layer shows lateral anomalies (at ca. 200, 320 and 400 m profile distance) corresponding to silty materials ($\rho < 20$ Ωm) which indicates a partially confined aquifer.

We observe an increase in the uncertainty of the layer thicknesses for deeper layers, as well as a larger uncertainty for layers associated with higher resistivity values. However, in the case of the fifth model-layer, we observe a lower standard deviation of the resistivity values for the common prior results, which might be related to a correlation between the resistivity of the fourth and fifth layer (see Fig. A3 in the appendix). This low standard deviation may be also a consequence of the TR approach and the choice

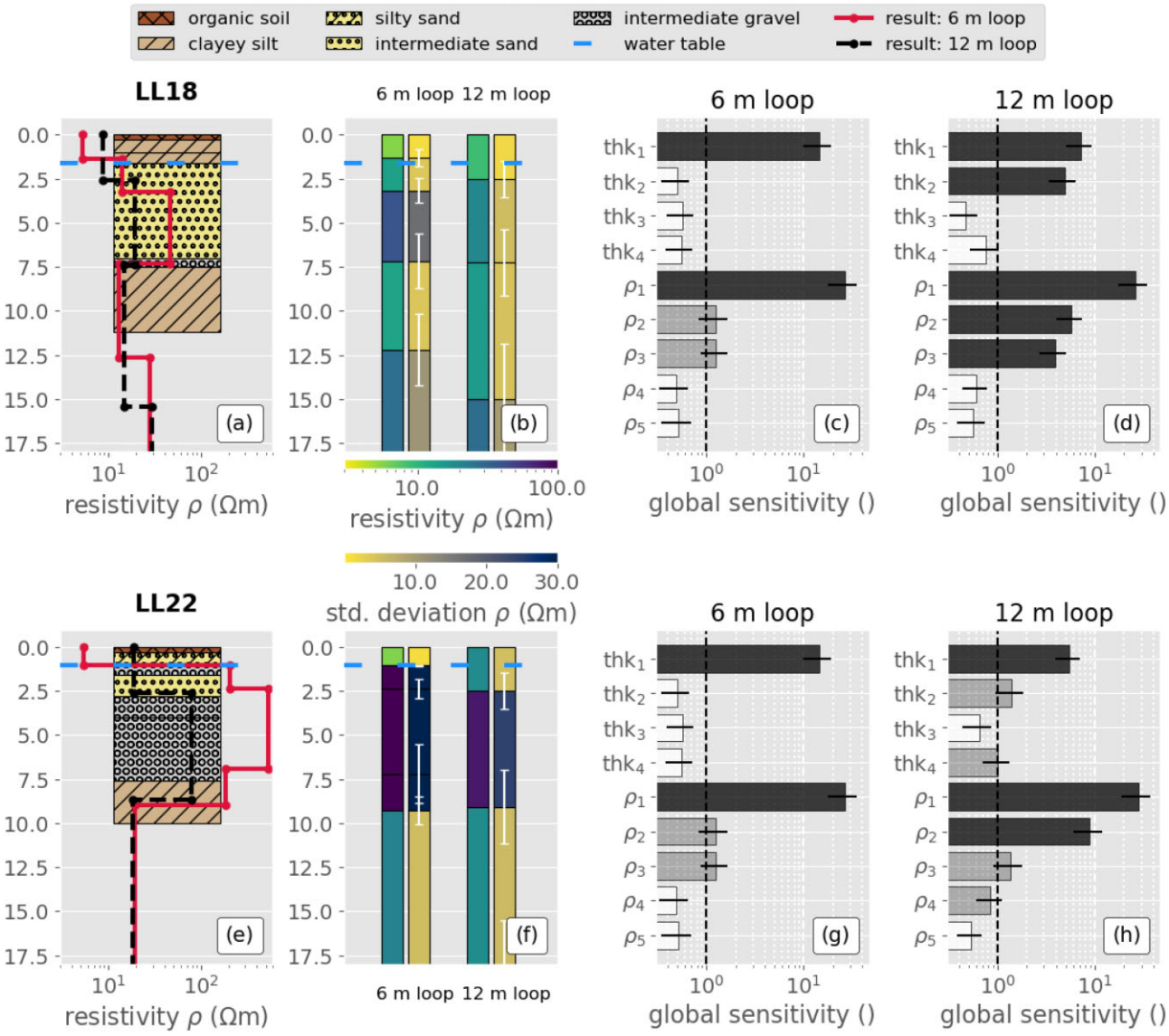

Figure 2. Direct comparison of borehole lithology to TEM results from a deterministic inversion and BEL1D. Results for borehole LL18 are shown in subplots a to d, while results of borehole LL22 are shown in subplots e to h. The uncertainty obtained from BEL1D is shown in b and f, where the colour bars are valid for all four logs, while the white error bars depict the single standard deviation of the layer thicknesses. The global sensitivity of the model parameters is shown in c, d, g and h, where dark bars indicate a sensitivity including the confidence interval above one, grey bars indicate a sensitivity that is statistically inconclusive whereas white bars are related to model parameters that are not sensitive to the model response.

of the prior space, which provides only an approximation of the posterior uncertainty. The comparison of stochastic results from individual prior model spaces (Figs 4b, c) to those from a common prior model space (Figs 4d, e) reveals that both approaches solve in general for the same three layer subsurface model. The common prior approach (Figs 4d, e), however, solves for a smoother mean model laterally, while the individual prior approach solves for stronger lateral contrast, as well as for a larger range in resistivity values (i.e. lower minimum and higher maximum resistivity). We observe that the resistivity values in the conductive (i.e. third) layer are more consistent laterally in the common prior result (Fig. 4d) than for the individual prior result (Fig. 4b). The lateral variability in the first and second layers, however, is reduced compared to the lateral resistivity contrast in the deterministic (Fig. 4a) and the stochastic inversion result from individual prior models (Figs 4b, c).

Histograms of the electrical resistivity (Fig. 5) reveal that the results from a common prior vary in a narrower range (ca. 15 to 34 Ωm), compared to the results from both the deterministic inversion and the individual priors (ca. 12 to 38 Ωm). The distribution of the electrical resistivity from the individual prior result (Fig. 5a) is left-skewed, while the distribution of the electrical resistivity from the common prior result (Fig. 5a) is bi-modal. The contrast between high and low electrical resistivity remains large enough to ensure sufficient contrast to discriminate between layers as the majority of the standard deviation of electrical resistivity is below 12 Ωm (see Figs 6a and b). However, in the case of the common prior result, we observe separated bins (Fig. 6b) compared to the

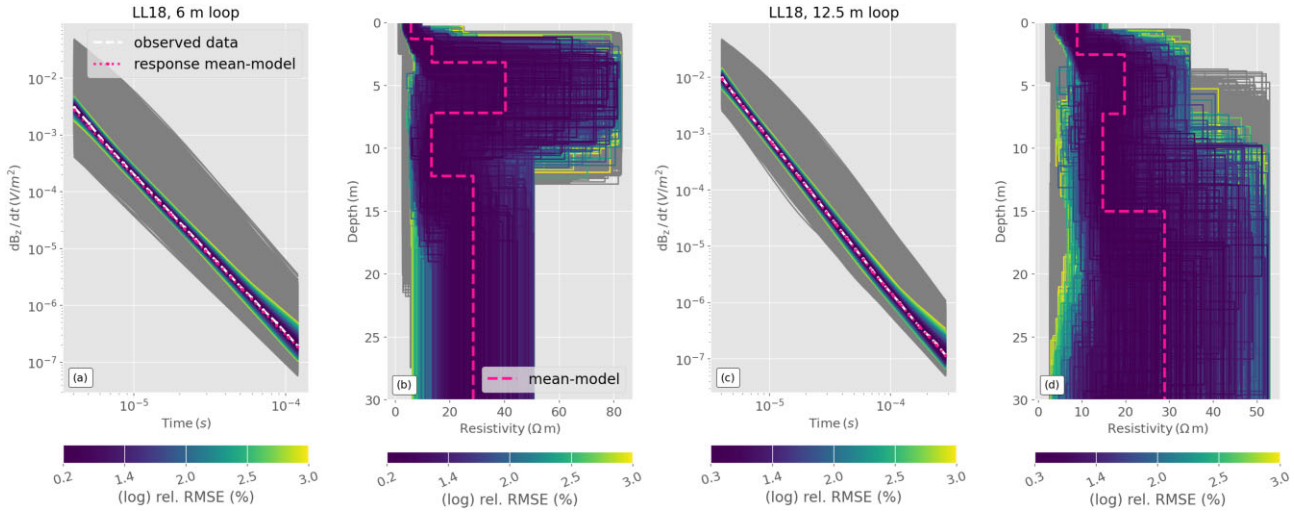

Figure 3. Stochastic inversion results from TEM data measured at borehole LL18 using a 6.25 m (a, b) and a 12.5 m (c, d) square single loop. Prior data and model spaces are shown in grey in the background, while the coloured lines represent the posterior data and model spaces.

right-skewed distribution of the individual prior result (Fig. 6a). The uncertainty of the resistivity is similar for both approaches, ranging between 3 Ωm for conductive layers and 12 Ωm for resistive layers (see Figs 6a and d). The uncertainty of the layer thickness is also similar for both prior model versions ranging between ca. 1.0 m for shallow layers and ca. 7.0 m for deep layers (see Figs 6c and d).

The area (i.e. volume for a unit width in vertical direction m^3/m) associated to the first aquifer amounts to ca. 20.000 m^2 with an uncertainty range of ca. 16.000 m^2 to ca. 28.000 m^2 (derived from the one fold standard deviation of the upper and lower layer uncertainty) and we obtain a depth to the shallow aquifer of ca. 3.0 m and an uncertainty of 1.0 m. The second aquifer is located in a depth of ca. 25.0 m with an uncertainty of 5.0 m. These quantification of the aquifer geometry is independent of the prior model approach, demonstrating that the common prior approach is capable of quantitatively retrieving the same aquifer geometry as individual priors for each sounding. Moreover, the common prior approach increases the consistency between the electrical units of adjacent units. The common prior approach requires a computational time reduced by 65 per cent compared to the individual prior (544 to 1532 min), due to a reduction of the required forward model runs (570 000 instead of 1620 000).

3.3 Numerical data experiment to compare the uncertainty estimation from individual prior models to a single common prior model for inversion of soundings along a 2-D section

We have established the accuracy of BEL1D to resolve lithological contacts by comparing the stochastic results to borehole data. Additionally, we demonstrated for a laterally homogeneous subsurface that a common prior model can resolve the same electrical units as a deterministic inversion and a stochastic inversion using individual priors for each sounding. We are now investigating whether the common prior approach can resolve for strong lateral contrasts. To this end, we conduct a numerical experiment, along a short profile with known lateral heterogeneities. Fig. 7 shows the numerical models, associated forward model responses and the corresponding global sensitivity calculated with the DGSA methodology. The numerical model represents a three layer lithology, with the second layer corresponding to the aquifer. In general, we observe higher global sensitivity for model parameters close to the surface (i.e. resistivity and thickness of the first layer). The thickness of the first layer shows a higher global sensitivity than the thicknesses of the second layer (i.e. the aquifer). The DGSA results show an inconclusive global sensitivity for the resistivity of the second layer and demonstrate that the data is not sensitive to the resistivity of the third layer. The thickness of the second layer is non-influential on the model response for sounding positions T02, T03 and T04, while the global sensitivity of the second layer is slightly higher (but statistically still inconclusive) at sounding positions T01 and T05.

Fig. 8 shows a 2-D model built from the results obtained with the deterministic inversion (Fig. 8a) and stochastic inversion using individual prior model spaces for each sounding (Figs 8b and c) and using a common prior model space for all soundings (Figs 8d and e). The stochastic inversion results are visualized in terms of the mean (Figs 8b and d) and the standard deviation (Figs 8c and e) of the posterior distribution (thickness and resistivity). In general, we observe for all sounding positions an increase in the uncertainty of the layer thicknesses for deeper layers, as well as a larger uncertainty for the resistivity of the second layer, due to its higher resistivity values. The deterministic inversion solves for thickness values close (i.e. ca. $\pm$ 2 m) to their respective true interface depths. The only exception is sounding position T04, where we can observe a clear underestimation of the depth to the aquifer by ca. 3 m. We observe a similar bias in the mean of the stochastic inversion result (Figs 8b and c) that was obtained from individual priors, because the prior model space was centred on the deterministic inversion result. Stochastic inversion results using the common prior model space at sounding position T04 reveal an exact retrieval of the first layer thickness and the uncertainty (Fig. 8e) indicates that the data can be also explained by a first layer that is 3 m thinner or thicker.

The comparison between stochastic inversion results obtained from individual priors for each sounding position (Figs 8b and c) to those obtained from a common prior for all sounding positions

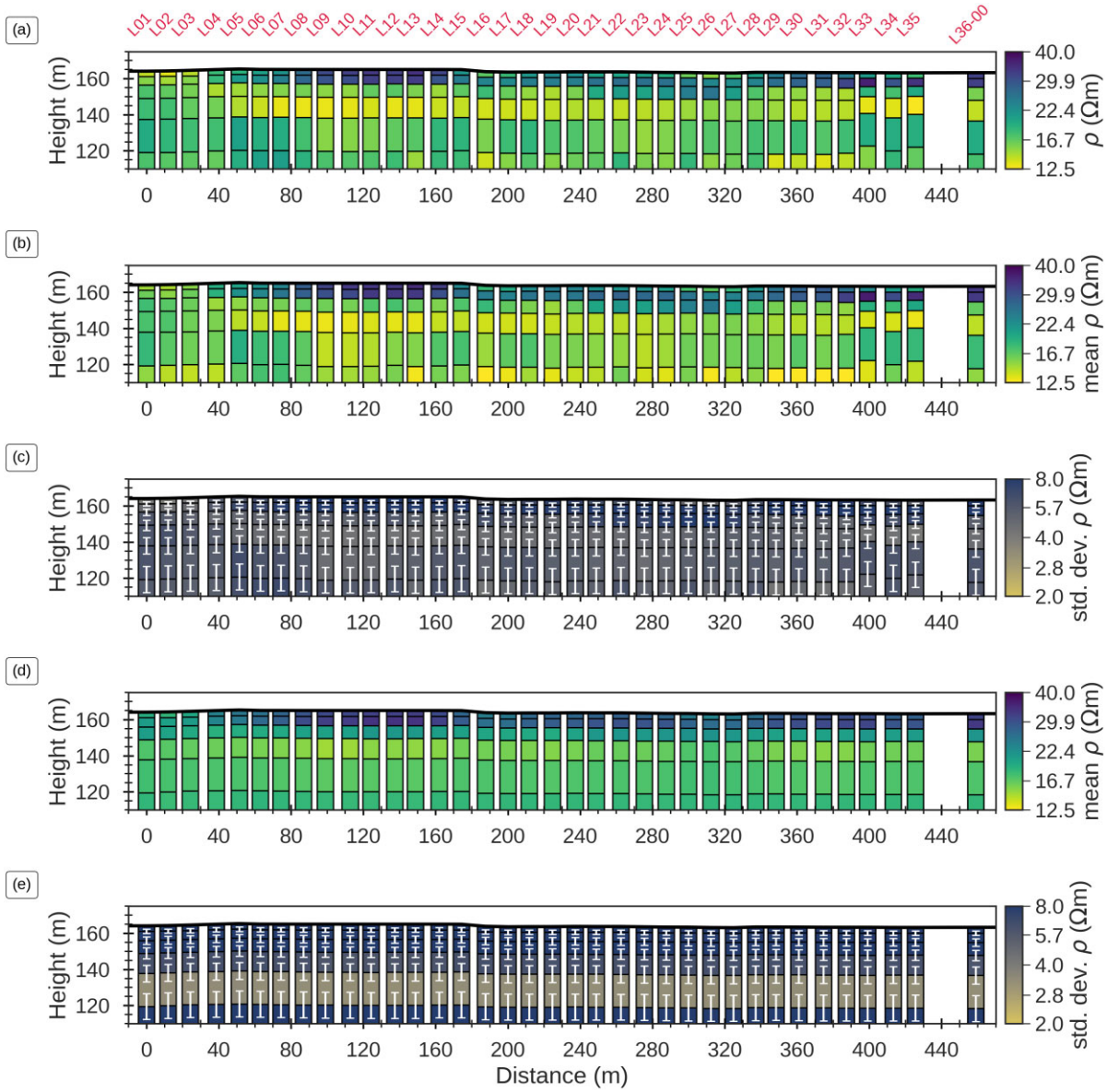

Figure 4. Results from deterministic inversion (a) and BEL1D (b to e) for field TEM data collected at the soda lakes. The mean resistivity of the posterior distribution is shown in b for individual prior model spaces for each sounding and in d for a common prior model space used to estimate the posterior of all five soundings. The standard deviation of the posterior distribution is shown in c and e, where the white error bars indicate the single standard deviation of the layer thicknesses.

(Figs 8d and e) reveals mainly consistent results, indicating that both approaches estimate an adequate posterior distribution of the model parameters. However, the uncertainty of the layer thickness obtained from the common prior is ca. 10 per cent larger than for the individual priors, while the uncertainty of the layer resistivity is similar for both prior model approaches. The large (i.e. > 5 m) uncertainty associated with the layer thicknesses in the case of the common prior results can be attributed to the wider prior model space. In particular, we observe that the layer thickness is overestimated at sounding positions T01 and T05. Hence, the wider prior model space results in a lateral smoothing of the obtained resistivity values, yet the uncertainty range (one standard deviation, see Fig. 8e) shows that the true model lies within the solved posterior model space, except for the first layer thickness at sounding position T01 and the second layer thickness at sounding position T05. Sounding positions T01 and T05 are related to the smallest first layer thickness, which is overestimated by the common prior results because these small first layer thicknesses are at the edge of the common prior model space. In comparison, the mean of the posterior distribution obtained from individual prior models for soundings T01 and T05 resolve the true model values slightly better than the common prior solution resulting in a slightly larger uncertainty. This is plausible because the larger uncertainty in the common prior approach is associated to the variability of the deterministic solutions. Additionally, due to the TR approach, all models in the posterior fit the data. This result mainly highlights that stochastic approaches are relying on a careful definition of the prior.

Fig. 9 shows a comparison of the posterior correlation for the individual and the common prior at sounding position T03. The histograms in the main diagonal of Fig. 9 reveal that both prior

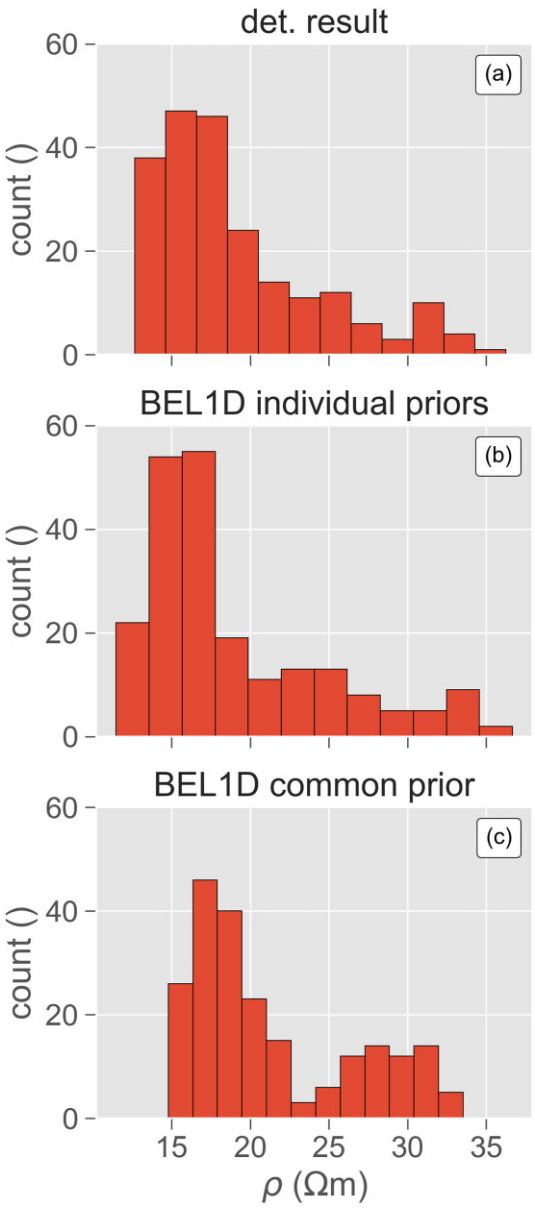

Figure 5. Histograms of the resulting mean resistivity distributions (for all layers) obtained from the deterministic inversion (a), stochastic inversion with individual priors for each sounding (b) and stochastic inversion with a common prior for all soundings (c).

spaces result in similar posterior distributions that estimate the true model values with minor deviation for the thickness and resistivity of the second layer. In the case of the thickness, both approaches overestimate the thickness by ca. 20 per cent. The fourth histogram in the main diagonal of Fig. 9 corresponds to the resistivity of the second layer and reveals that both approaches (in terms of the mean posterior distribution) underestimate the resistivity by ca. 50 per cent. Furthermore, we observe a weak logarithmic correlation between the thickness and resistivity of the first layer. Fig. A4 (in appendix) shows the same visualization at sounding position T01 and indicates that the common prior approach might result in a bias in the case of a true model that lies at the edge of the prior model

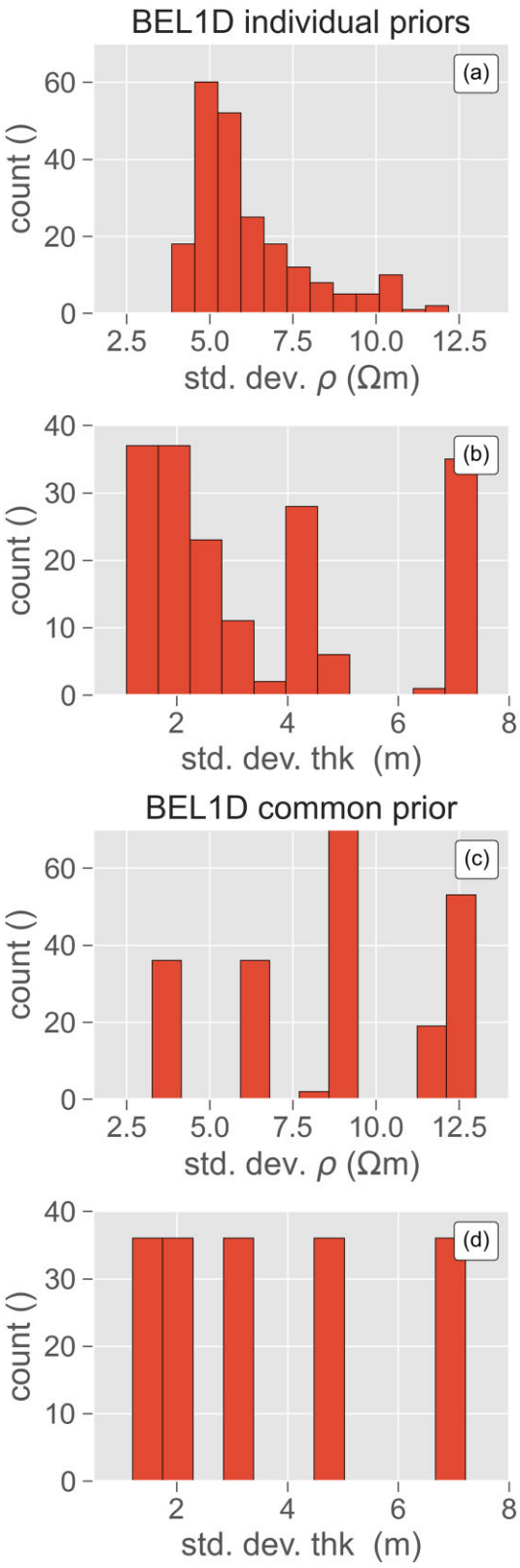

Figure 6. Histograms of the standard deviations for the resistivity (a and b) and the thickness (c and d) individual priors for each sounding (a and c) and a common prior for all soundings (b and d).

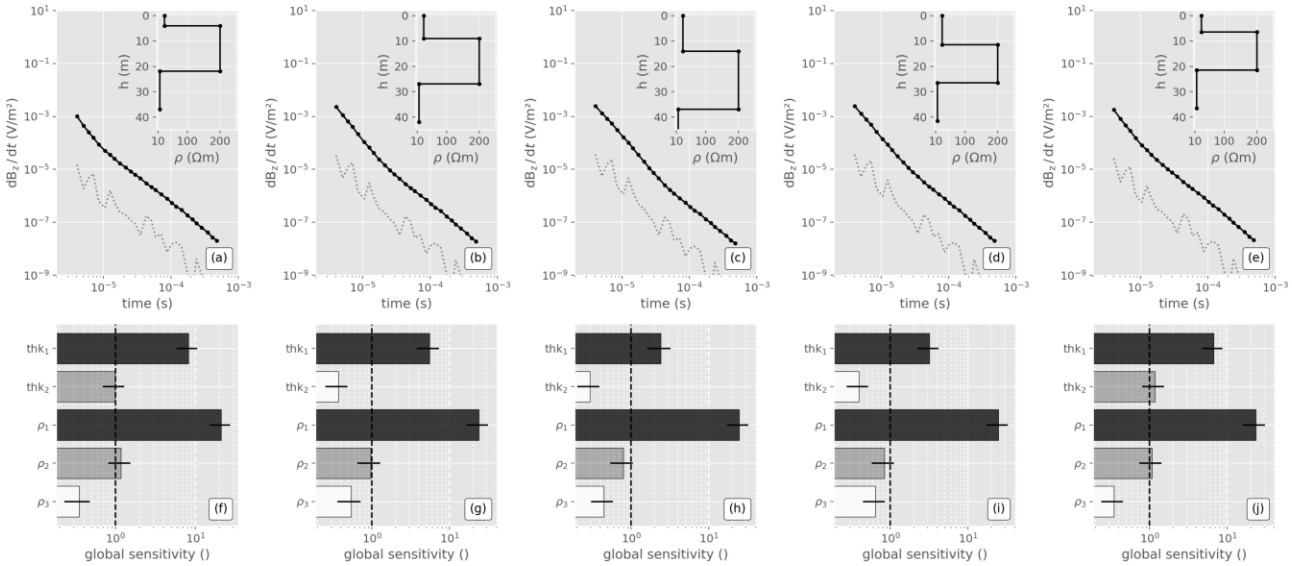

Figure 7. Numerical models, forward modelled data and numerical error (grey dotted line in (a) to (e), as well as the corresponding model parameter sensitivities in (f) to (j). The vertical dashed line indicates the threshold of 1 (i.e. larger sensitivities indicate influential parameters) and the horizontal black lines the confidence interval of the corresponding sensitivity. Black bars in (f) to (j) indicate influential model parameters, white bars non-influential parameters and grey bars indicate model parameters with a statistically inconclusive sensitivity.

space, because the prior is not centred on the true model values. This is an indication that the results remain sensitive to the choice of the prior.

Both the common and the individual prior approaches obtain the true model values within one standard deviation, yet, the common prior approach requires a reduced computational time by 51 per cent (75 to 155 min). This reduction is directly related to the number of forward calculations that are required to obtain an approximation of the posterior distribution. In the case of the individual prior results (Figs 8b and c) we ran 150 000 forward calculations (30 000 for each sounding) to obtain the prior model space. Additionally, we required 75 000 forward calculations to obtain the posterior distributions resulting in 225 000 forward calculations. In the case of the common prior, we ran only 30 000 forward calculations to obtain a single prior model space that we used to obtain the posterior distributions for each sounding (75 000 models for all soundings), which results in only 105 000 forward calculations.

4 DISCUSSION

Our numerical and field data experiments show the added value of using a stochastic inversion approach to determine the aquifer geometry and the associated uncertainty from TEM data. The successful application of stochastic inversion relies on an adequate selection of the prior model space (e.g. Scheidt *et al.* 2018). Hence, the posterior distribution is dependent on the choice of the prior model space which is inherent to any stochastic method (e.g. Ahmed *et al.* 2024). In theory, the prior model space should represent all knowledge before acquiring data on the field and it is generally recommended to be as large as possible. Large prior spaces, however, tend to result in larger estimated uncertainties and require more samples for the learning phase, and thus, increase the computation time. Additionally, in large prior spaces, the relationship between data any model space becomes increasingly nonlinear, which may limit the applicability of the CCA method and might require more advanced approaches to map the data-model relationship in the future (e.g. Thibaut 2023). We propose here a pragmatic approach that combines a deterministic inversion with a subsequent stochastic inversion. In particular, we evaluate an efficient estimation of the posterior model space for multiple TEM soundings from a common prior space which is based on deterministic solutions of each sounding.

In a first step, we showed that the TEM results from single sounding positions correspond to geological data obtained from two shallow boreholes, showing that high electrical resistivity ($>50\ \Omega$m) are associated with sandy gravel aquifers, whereas low electrical resistivity ($<15\ \Omega$m) are associated with aquicludes consisting of clayey silts. We also showed that the sensitivity of the TEM method depends on the loop size, demonstrating that an increase of the loop size results in a sensitivity loss close to the surface, yet it improves the sensitivity and the delineation of deep interfaces. The comparison between the TEM results from both a deterministic and stochastic inversion approach correspond well to the lithology obtained from the two shallow boreholes, demonstrating that the TEM method is capable of resolving the aquifer geometry while also providing the uncertainty of the derived interfaces. Our study shows that the forward modeller proposed by Aigner *et al.* (2024) can be implemented into the pyBEL1D framework (Michel *et al.* 2023) to obtain a stochastic inversion of TEM data resolving the resistivity values and thickness of subsurface materials, as well as their associated uncertainties. We also demonstrate that deterministic and stochastic inversions provide consistent results. While the former permits a fast analysis, they do not provide rigorous information about the accuracy of the model parameters. The stochastic inversion permits to solve for the uncertainty, but requires an increased computational time compared to the deterministic inversion. Choosing the prior space based on deterministic inversion results

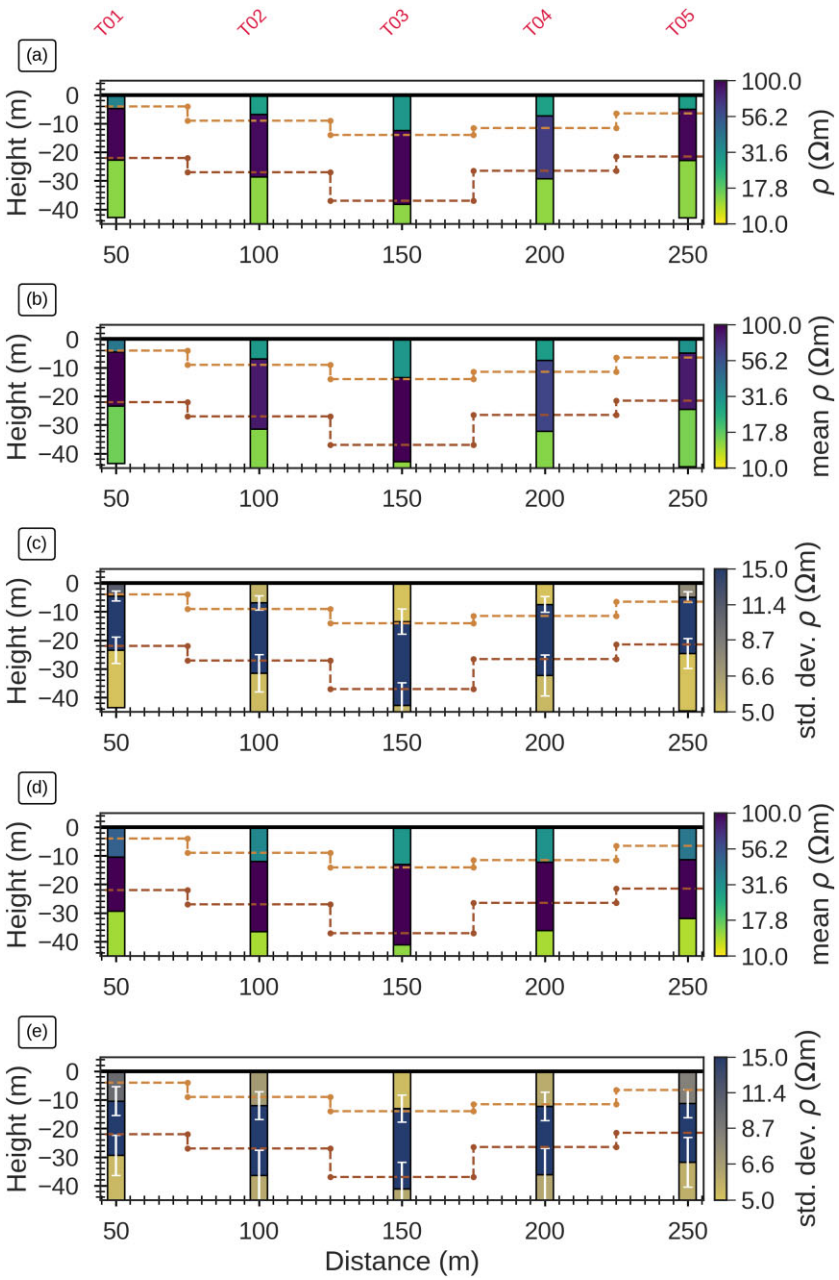

Figure 8. Results from deterministic inversion (a) and BEL1D (b to e) for numerical TEM data. The mean resistivity of the posterior distribution is shown in (b) for individual prior model spaces for each sounding and in (d) for a common prior model space used to estimate the posterior of all five soundings. The standard deviation of the posterior distribution is shown in (c) and (e), where the white error bars indicate the single standard deviation of the layer thicknesses. The dashed lines indicate the true model interfaces of the numerically modelled aquifer that is confined between two conductive units.

is adequate to approximate the posterior model space as there is an effective reduction of uncertainty over most model parameters (see Fig. 3). In the case of parameters where no uncertainty reduction is observed, we recommend to increase the prior space (e.g. $\pm 1/3$ or $\pm 1/2$)

In a second step, we investigate the use of a common prior to obtain the uncertainty of multiple TEM soundings from a single large prior model space. In particular, we showed that a common prior model derived from the minimum and maximum values of all individual deterministic results resolves the interfaces and associated uncertainties of 36 TEM soundings at the field. Our results demonstrate that in case of small lateral variations, the common prior solution solves for equal models as the deterministic solution and the stochastic solution using individual prior models. Additionally, the common prior solution has the advantage of solving for laterally consistent models at depth, effectively leveraging the common prior information to overcome the reduced sensitivity of our TEM configuration at depth without overly smoothing the shallow parts of the model where the sensitivity of our TEM configuration is much higher.

In a third step, we investigate the common prior approach in a numerical experiment with significant lateral variations. In this case,

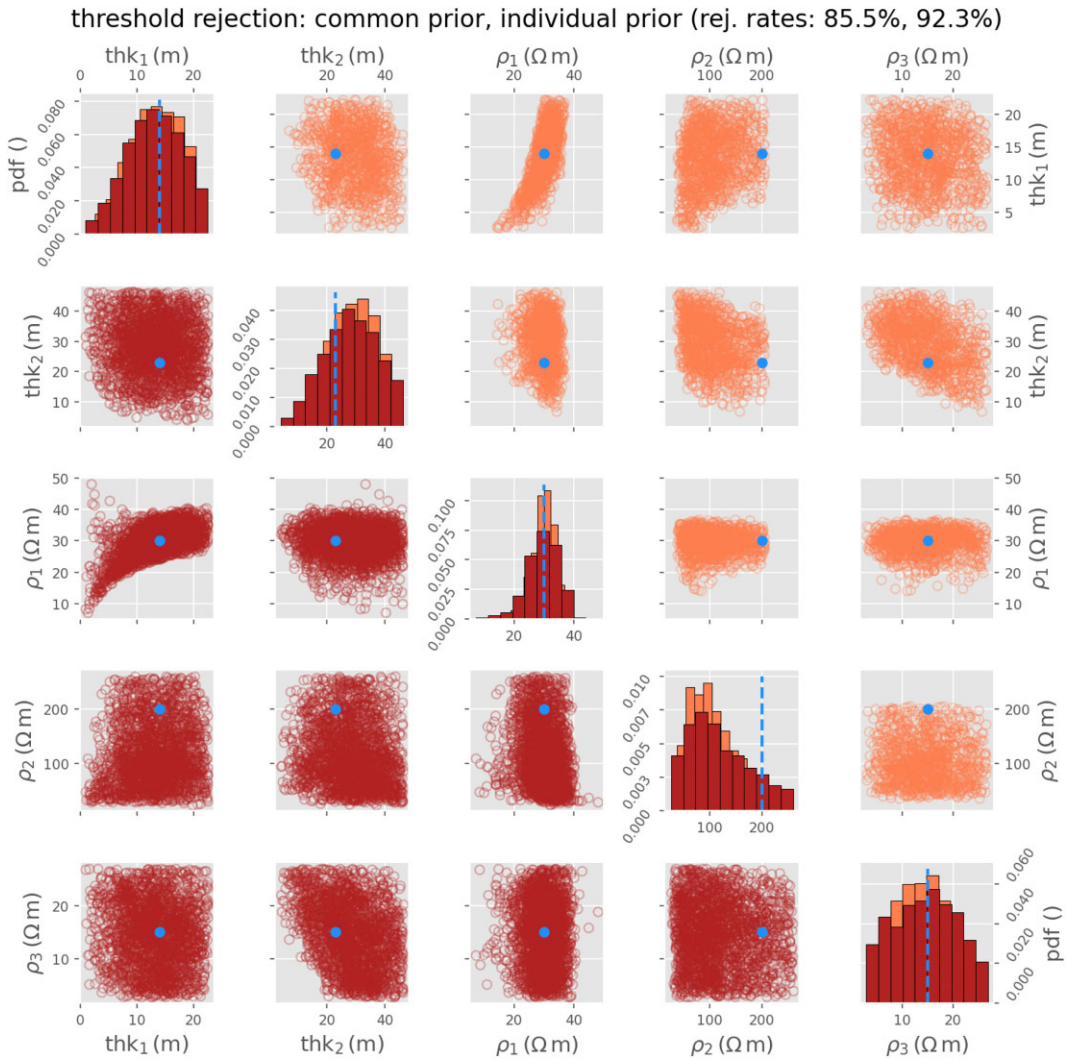

Figure 9. Correlation visualization of the posterior model space for sounding T03. The main diagonal shows the probability density for each model parameter and the orange bars correspond to the individual prior results while the red bars correspond to the common prior result. The right triangular entries (light orange circles) show the model parameter correlations for all parameter combinations in model units [thk (m), ρ (Ωm)] corresponding to the individual prior result. The left triangular entries (dark red circles) show the model parameter correlations for all parameter combinations in model units [thk (m), ρ (Ωm)] corresponding to the common prior result. The blue dashed line and the blue solid dots indicate the values of the true model.

we demonstrate a limitation of the common prior approach and show that the individual prior model solution solves such strong lateral changes better than the common prior approach. This highlights the advantage of using our approach that combines deterministic and stochastic inversion strategies because sole application of the deterministic inversion delivers only a linearized estimation of uncertainty based on the Jacobian matrix, while sole application of a stochastic inversion using a large prior model might result in the loss of lateral resolution. The estimated uncertainty corresponds well to the model parameters sensitivity derived from DGSA showing that layers with high electrical resistivity are associated with a large uncertainty and low sensitivities, whereas layers with a low electrical resistivity are associated with a small uncertainty and high sensitivities.

Recent developments in instrumentation and field methodologies allow for quasi-continuous TEM data collection in both ground-based (e.g. Auken *et al.* 2018 and Street *et al.* 2018) and waterborne studies (e.g. Lane *et al.* 2020; Yogeshwar *et al.* 2020; Bücker *et al.* 2021 and Aigner *et al.* 2021). Such instruments are capable of collecting hundreds of soundings per day that are commonly inverted using approaches with limited uncertainty quantification. Estimation of the model parameter uncertainty based on McMC approaches (e.g. Minsley 2011) for such a massive number of soundings would be computational too expensive. Hence, the added value of the common prior space solution compared to a solution based on individual prior model spaces lies in a reduction (65 per cent) of the computation time for the 36 soundings collected at our field site. This reduction originates largely from the number of required forward simulations that is greatly reduced in the common prior approach, as the forward modelling for the prior samples must only be run once and only the posterior sampling and subsequent forward modelling must be run for each sounding. The reduction

in computation time, therefore, scales with the number of soundings, an improvement over more traditional stochastic approaches. Furthermore, the common prior result is laterally more consistent at depth than the solutions from the deterministic inversion and the individual priors, yet as shown in the numerical experiment, this might be problematic in the case of large lateral heterogeneities.

This work provides added value for future studies which require geophysical data to inform groundwater model either in terms of geometry (e.g. Hermans *et al.* 2015) or of processes (e.g. Perzan *et al.* 2021). In coupled inversion approaches (e.g. Hinnell *et al.* 2010), the link between geophysical and hydrogeological parameters is through a petrophysical relationship (Irving & Singha 2010), which prevents the explicit inversion of geophysical data. However, applying it in practice would often make the hydrogeological model more complex than necessary. For example, a model of a confined aquifer constrained by TEM data should include a shallow aquifer and the unsaturated zones as they impact the geophysical response. Therefore, sequential approaches where geophysical inversion results are used to constrain the geometry of the hydrological model are still highly relevant. Recently, Enemark *et al.* (2024) proposed a methodology to assess the impact of geological uncertainty on hydrogeological model predictions. The uncertainty of the geological scenarios integrates an uncertainty component originating from the interpretation of a deterministic inversion model from airborne EM data (published in Møller *et al.* 2009) obtained with the SkyTEM system (Sørensen & Auken 2004). Such uncertainty integration necessarily includes a subjective component related to the expert who provided an estimation of uncertainty. If the geophysical data were inverted stochastically, the geological uncertainty estimation can be done in a fully probabilistic framework (e.g. Hermans *et al.* 2015; Scheidt *et al.* 2018; Michel *et al.* 2023). Our study provides the foundation for such future approaches that require the efficient uncertainty estimation from TEM data.

5 CONCLUSION

We demonstrated that the stochastic inversion approach can be used to efficiently estimate the uncertainty associated with TEM soundings using numerical and field data experiments. To this end, we combined open-source modelling and inversion routines with the open-source package pyBEL1D. In particular, we use a combined approach that is based on an initial deterministic inversion to generate an informed prior model space, which is then used in the stochastic framework to estimate the uncertainty of the model parameters (i.e. thickness and resistivity). The stochastic inversion with BEL1D offers the advantage that the posterior distribution of multiple TEM soundings can be estimated from a single prior model space, which drastically reduces the computational time for multiple soundings. In a first step, we demonstrated that the deterministic and stochastic results correspond with borehole data, associated to two aquifers. Low electrical resistivity values ($<15\ \Omega$m) correspond to fine grain sediments confining the aquifer, which is associated with high electrical resistivity values ($>30\ \Omega$m). In a second step, we investigate TEM data of 36 TEM soundings collected along a profile and directly estimate the posterior model distributions as well as the associated uncertainty to derive the aquifer geometry at the soda lakes test site. Our results show that the common prior derives similar laterally homogeneous electrical units as the deterministic solution and estimates similar uncertainties as the individual prior solution. Additionally, the common prior solution is laterally more consistent along the profile than the solution based on individual prior model spaces for each sounding while reducing the computational time by 65 per cent. In a third step, we investigated in a numerical experiment associated to a confined aquifer with lateral thickness variations, whether the common prior is capable of retrieving such strong lateral variations. Our results revealed that, in case of strong lateral variability, the individual prior solution retrieves the true models slightly better than the common prior solution, yet both approaches resolve the true model values within one standard deviation of the mean model. These findings offer the added value of efficient uncertainty estimation as required for applications using TEM system that are capable of continuously collecting huge data sets, which are essential to obtain the uncertainty associated to aquifer system at large scales with a high lateral resolution.

ACKNOWLEDGMENTS

We gratefully acknowledge the Editor Lindsey J. Heagy and two anonymous reviewers for their insightful comments that helped to improve the manuscript substantially. We would like to thank Anna Hettegger, Nathalie Roser, Clemens Moser and Luzian Wolf for helping with the field work. Additionally, we are grateful to Arno Cimadom and all National Park Neusiedlersee employees for allowing the measurements on their protected areas and help with logistics. We acknowledge TU Wien Bibliothek for financial support through its Open Access Funding Programme. Parts of this work were funded by the LIFE22-NAT-AT-LIFE Pannonic 'Salt-Restoration and preservation of Pannonic salt lakes and salt steppes of European significance' (Project 101113569) which was funded by the LIFE Programme.

CONFLICT OF INTEREST

The authors declare that they have no known competing financial interests or personal relationships that could have appeared to influence the work reported in this paper.

DATA AVAILABILITY

All data, scripts and Python modules necessary to reproduce the results can be found at https://doi.org/10.48436/z8ejc-sec60 hosted at the TU Wien. Additionally, we added changes to pyBEL1D to a new branch in the corresponding GitHub repository (https://github.com/hadrienmichel/pyBEL1D/tree/tem).

REFERENCES

Ahmed, A., Aigner, L., Michel, H., Deleersnyder, W., Dudal, D., Flores Orozco, A. & Hermans, T., 2024. Assessing and improving the robustness of Bayesian evidential learning in one dimension for inverting time-domain electromagnetic data: Introducing a new threshold procedure, *Water,* **16**(7), doi:10.3390/w16071056.

Aigner, L., Högenauer, P., Bücker, M. & Flores Orozco, A., 2021. A flexible single loop setup for water-borne transient electromagnetic sounding applications, *Sensors,* **21**(19), 6624, doi:10.3390/s21196624.

Aigner, L., Werthmüller, D. & Flores Orozco, A., 2024. Sensitivity analysis of inverted model parameters from transient electromagnetic measurements affected by induced polarization effects, *Journal of Applied Geophysics,* **223,** 105334, doi:10.1016/j.jappgeo.2024.105334.

Aster, R.C., Borchers, B. & Thurber, C.H., 2005. *Parameter Estimation and Inverse Problems, vol. 90 of* ***International geophysics series,*** Elsevier Science & Technology, San Diego, 1st edn.

Aster, R.C., Borchers, B. & Thurber, C.H., 2018. *Parameter Estimation and Inverse Problems,* Elsevier.

Atekwana, E.A. & Atekwana, E.A., 2010. Geophysical signatures of microbial activity at hydrocarbon contaminated sites: a review, *Surv. Geophys.,* **31,** 247–283.

Auken, E., Jørgensen, F. & Sørensen, K.I., 2003. Large-scale TEM investigation for groundwater, *Explor. Geophys.,* **34**(3), 188–194.

Auken, E. *et al.*, 2015. An overview of a highly versatile forward and stable inverse algorithm for airborne, ground-based and borehole electromagnetic and electric data, *Explor. Geophys.,* **46**(3), 223–235.

Auken, E., Foged, N., Larsen, J.J., Lassen, K.V.T., Maurya, P.K., Dath, S.M. & Eiskjær, T.T., 2018. tTEM—a towed transient electromagnetic system for detailed 3D imaging of the top 70 m of the subsurface, *Geophysics,* **84**(1), E13–E22.

Ball, L.B., Bedrosian, P.A. & Minsley, B.J., 2020. High-resolution mapping of the freshwater–brine interface using deterministic and Bayesian inversion of airborne electromagnetic data at Paradox Valley, USA, *Hydrogeol. J.,* **28**(3), 941–954.

Binley, A., Hubbard, S.S., Huisman, J.A., Revil, A., Robinson, D.A., Singha, K. & Slater, L.D., 2015. The emergence of hydrogeophysics for improved understanding of subsurface processes over multiple scales, *Water Resour. Res.,* **51**(6), 3837–3866.

Blatter, D., Key, K., Ray, A., Foley, N., Tulaczyk, S. & Auken, E., 2018. Trans-dimensional Bayesian inversion of airborne transient EM data from Taylor glacier, Antarctica, *Geophys. J. Int.,* **214**(3), 1919–1936.

Bücker, M. *et al.*, 2021. Integrated land and water-borne geophysical surveys shed light on the sudden drying of large Karst lakes in southern Mexico, *Solid Earth,* **12**(2), 439–461.

Cassiani, G. *et al.*, 2014. Noninvasive characterization of the Trecate (Italy) crude-oil contaminated site: links between contamination and geophysical signals, *Environ. Sci. Pollut. Res.,* **21,** 8914–8931.

Christiansen, A.V. & Auken, E., 2012. A global measure for depth of investigation, *Geophysics,* **77**(4), WB171–WB177.

Christiansen, A.V., Auken, E. & Sørensen, K., 2006. The transient electromagnetic method, in *Groundwater geophysics,* pp 179–225, Springer.

Cong-Thi, D., Dieu, L.P., Thibaut, R., Paepen, M., Ho, H.H., Nguyen, F. & Hermans, T., 2021. Imaging the structure and the saltwater intrusion extent of the luy river coastal aquifer (Binh Thuan, Vietnam) using electrical resistivity tomography, *Water,* **13**(13), 1743, doi:10.3390/w13131743.

Danielsen, J.E., Auken, E., Jørgensen, F., Søndergaard, V. & Sørensen, K.I., 2003. The application of the transient electromagnetic method in hydrogeophysical surveys, *J. Appl. Geophys.,* **53**(4), 181–198.

Deleersnyder, W., Maveau, B., Hermans, T. & Dudal, D., 2023. Flexible quasi-2d inversion of time-domain aem data, using a wavelet-based complexity measure, *Geophys. J. Int.,* **233**(3), 1847–1862.

Enemark, T. *et al.*, 2024. Incorporating interpretation uncertainties from deterministic 3D hydrostratigraphic models in groundwater models, *Hydrol. Earth System Sci.,* **28**(3), 505–523.

Fenwick, D., Scheidt, C. & Caers, J., 2014. Quantifying asymmetric parameter interactions in sensitivity analysis: application to reservoir modeling, *Math. Geosci.,* **46**(4), 493–511.

Fitterman, D.V. & Stewart, M.T., 1986. Transient electromagnetic sounding for groundwater, *Geophysics,* **51**(4), 995–1005.

Fleckenstein, J.H., Krause, S., Hannah, D.M. & Boano, F., 2010. Groundwater-surface water interactions: new methods and models to improve understanding of processes and dynamics, *Adv. Water Resour.,* **33**(11), 1291–1295, Special Issue on ground water-surface water interactions.

Flores Orozco, A., Ciampi, P., Katona, T., Censini, M., Papini, M.P., Deidda, G.P. & Cassiani, G., 2021. Delineation of hydrocarbon contaminants with multi-frequency complex conductivity imaging, *Sci. Total Environ.,* **768,** 144997, doi:10.1016/j.scitotenv.2021.144997.

Goldman, M., Gilad, D., Ronen, A. & Melloul, A., 1991. Mapping of seawater intrusion into the coastal aquifer of Israel by the time domain electromagnetic method, *Geoexploration,* **28**(2), 153–174.

Grombacher, D., Maurya, P.K., Lind, J.C., Lane, J. & Auken, E., 2022. Rapid mapping of hydrological systems in Tanzania using a towed transient electromagnetic system, *Groundwater,* **60**(1), 35–46.

Guérin, R., Descloitres, M., Coudrain, A., Talbi, A. & Gallaire, R., 2001. Geophysical surveys for identifying saline groundwater in the semi-arid region of the Central Altiplano, Bolivia, *Hydrol. Process.,* **15**(17), 3287–3301.

Heagy, L.J., Cockett, R., Kang, S., Rosenkjaer, G.K. & Oldenburg, D.W., 2017. A framework for simulation and inversion in electromagnetics, *Comput. Geosci.,* **107,** 1–19.

Hermann, H., 2023. Zur hydrogeologie der schwebenden grundwasserkörper unter den salzlacken des seewinkels (nördliches burgenland, Österreich)., *Berichte der GeoSphere Austria,* **145,** 152.

Hermans, T., Nguyen, F. & Caers, J., 2015. Uncertainty in training image-based inversion of hydraulic head data constrained to ERT data: Workflow and case study, *Water Resour. Res.,* **51**(7), 5332–5352.

Hermans, T., Oware, E. & Caers, J., 2016. Direct prediction of spatially and temporally varying physical properties from time-lapse electrical resistance data, *Water Resour. Res.,* **52**(9), 7262–7283.

Hermans, T., Nguyen, F., Klepikova, M., Dassargues, A. & Caers, J., 2018. Uncertainty quantification of medium-term heat storage from short-term geophysical experiments using Bayesian evidential learning, *Water Resour. Res.,* **54**(4), 2931–2948.

Hermans, T. *et al.*, 2023. Advancing measurements and representations of subsurface heterogeneity and dynamic processes: towards 4D hydrogeology, *Hydrol. Earth Syst. Sci.,* **27**(1), 255–287.

Hinnell, A., Ferré, T., Vrugt, J., Huisman, J., Moysey, S., Rings, J. & Kowalsky, M., 2010. Improved extraction of hydrologic information from geophysical data through coupled hydrogeophysical inversion, *Water Resour. Res.,* **46**(4), doi: 10.1029/2008WR007060.

Irving, J. & Singha, K., 2010. Stochastic inversion of tracer test and electrical geophysical data to estimate hydraulic conductivities, *Water Resour. Res.,* **46**(11), doi:10.1029/2009WR008340.

Kang, S., Knight, R. & Goebel, M., 2022. Improved imaging of the large-scale structure of a groundwater system with airborne electromagnetic data, *Water Resour. Res.,* **58**(4), e2021WR031439, e2021WR031439 2021WR031439.

Krzanowski, W.J., 2000. *Principles of Multivariate Analysis,* Oxford Univ. Press.

Lane, J.W. Jr *et al.*, 2020. Characterizing the diverse hydrogeology underlying rivers and estuaries using new floating transient electromagnetic methodology, *Sci. Total Environ.,* **740,** 140074, doi:10.1016/j.scitotenv.2020.140074.

Lindley, D.V., 1956. On a measure of the information provided by an experiment, *Ann. Math. Stat.,* **27**(4), 986–1005.

Meju, M., Fontes, S., Oliveira, M., Lima, J., Ulugergerli, E. & Carrasquilla, A., 1999. Regional aquifer mapping using combined ves-tem-amt/emap methods in the semiarid eastern margin of Parnaiba basin, Brazil, *Geophysics,* **64**(2), 337–356.

Michel, H., 2022. *pybel1d - a python implementation of bel1d,* Version 1.1.0. https://doi.org/10.5281/zenodo.6833249.

Michel, H., Nguyen, F., Kremer, T., Elen, A. & Hermans, T., 2020. 1D geological imaging of the subsurface from geophysical data with Bayesian evidential learning, *Comput. Geosci.,* **138,** 104456, doi:10.1016/j.cageo.2020.104456.

Michel, H., Hermans, T. & Nguyen, F., 2023. Iterative prior resampling and rejection sampling to improve 1-D geophysical imaging based on Bayesian Evidential learning (BEL1D), *Geophys. J. Int.,* **232**(2), 958–974.

Minsley, B.J., 2011. A trans-dimensional Bayesian Markov Chain Monte Carlo algorithm for model assessment using frequency-domain electromagnetic data, *Geophys. J. Int.,* **187**(1), 252–272.

Minsley, B.J., Foks, N.L. & Bedrosian, P.A., 2021. Quantifying model structural uncertainty using airborne electromagnetic data, *Geophys. J. Int.,* **224**(1), 590–607.

Møller, I., Søndergaard, V.H. & Jørgensen, F., 2009. Geophysical methods and data administration in danish groundwater mapping, *GEUS Bull.,* **17,** 41–44.

Nabighian, M.N., 1979. Quasi-static transient response of a conducting half-space—an approximate representation, *Geophysics,* **44**(10), 1700–1705.

Nabighian, M.N., *et al.*, 1991. Time domain electromagnetic prospecting methods, *Electromag. Methods Appl. Geophys.,* **2**(Part A), 427–509.

Ntona, M.M., Busico, G., Mastrocicco, M. & Kazakis, N., 2022. Modeling groundwater and surface water interaction: an overview of current status and future challenges, *Sci. Total Environ.,* **846,** 157355, doi:10.1016/j.scitotenv.2022.157355.

Paepen, M., Hanssens, D., De Smedt, P., Walraevens, K. & Hermans, T., 2020. Combining resistivity and frequency domain electromagnetic methods to investigate submarine groundwater discharge in the littoral zone, *Hydrol. Earth Syst. Sci.,* **24**(7), 3539–3555.

Perzan, Z., Babey, T., Caers, J., Bargar, J. & Maher, K., 2021. Local and global sensitivity analysis of a reactive transport model simulating floodplain redox cycling, *Water Resour. Res.,* **57**(12), e2021WR029723, doi:10.1029/2021WR029723.

Ray, A., Ley-Cooper, Y., Brodie, R.C., Taylor, R., Symington, N. & Moghaddam, N.F., 2023. An information theoretic Bayesian uncertainty analysis of AEM systems over Menindee Lake, Australia, *Geophys. J. Int.,* **235**(2), 1888–1911.

Rücker, C., Günther, T. & Wagner, F.M., 2017. pyGIMLi: An open-source library for modelling and inversion in geophysics, *Comput. Geosci.,* **109,** 106–123.

Scales, J.A. & Snieder, R., 1997. To Bayes or not to Bayes?, *Geophysics,* **62**(4), 1045–1046.

Scheidt, C., Renard, P. & Caers, J., 2015. Prediction-focused subsurface modeling: investigating the need for accuracy in flow-based inverse modeling, *Math. Geosci.,* **47,** 173–191.

Scheidt, C., Li, L. & Caers, J., 2018. *Quantifying Uncertainty in Subsurface Systems,* vol. **236,** John Wiley & Sons.

Schulze-Makuch, D., Carlson, D.A., Cherkauer, D.S. & Malik, P., 1999. Scale dependency of hydraulic conductivity in heterogeneous media, *Groundwater,* **37**(6), 904–919.

Singha, K. & Navarre-Sitchler, A., 2022. The importance of groundwater in critical zone science, *Groundwater,* **60**(1), 27–34.

Sørensen, K.I. & Auken, E., 2004. Skytem–a new high-resolution helicopter transient electromagnetic system, *Explor. Geophys.,* **35**(3), 194–202.

Street, G., Duncan, A., Fullagar, P. & Tresidder, R., 2018. Loupe-a portable em profiling system, *ASEG Extended Abstr.,* **2018**(1), 1–3.

Strutz, D. & Curtis, A., 2023. Variational bayesian experimental design for geophysical applications: seismic source location, amplitude versus offset inversion, and estimating co2 saturations in a subsurface reservoir, *Geophys. J. Int.,* **236**(3), 1309–1331.

Tarantola, A., 2005. *Inverse Problem Theory and Methods for Model Parameter Estimation,* SIAM.

Thibaut, R., 2023. *Machine Learning for Bayesian Experimental Design in the Subsurface,* Ph.D. thesis, Ghent University.

Thibaut, R., Compaire, N., Lesparre, N., Ramgraber, M., Laloy, E. & Hermans, T., 2022. Comparing well and geophysical data for temperature monitoring within a Bayesian experimental design framework, *Water Resour. Res.,* **58**(11), e2022WR033045, doi:10.1029/2022WR033045.

Tikhonov, A.N. & Arsenin, V.Y., 1977. Solutions of ill-posed problems. *V. H. Winston*.

Trainor-Guitton, W. & Hoversten, G.M., 2011. Stochastic inversion for electromagnetic geophysics: practical challenges and improving convergence efficiency, *Geophysics,* **76**(6), F373–F386.

Vrugt, J.A. & Ter Braak, C.J.F., 2011. Dream$_{(D)}$: an adaptive Markov Chain Monte Carlo simulation algorithm to solve discrete, noncontinuous, and combinatorial posterior parameter estimation problems, *Hydrol. Earth Syst. Sci.,* **15**(12), 3701–3713.

Werthmüller, D., 2017. An open-source full 3d electromagnetic modeler for 1d vti media in python: empymod, *Geophysics,* **82**(6), WB9–WB19.

Winter, T.C., 2000. *Ground Water and Surface Water: A Single Resource,* Diane Publishing.

Yogeshwar, P. *et al.*, 2020. Innovative boat-towed transient electromagnetics—investigation of the furnas volcanic lake hydrothermal system, azores, *Geophysics,* **85**(2), E41–E56.

APPENDIX A: APPENDIX

Fig. A1 shows the deterministic and stochastic inversion results for TEM soundings at the position of two boreholes, each for three different loop sizes. The stochastic inversion results are represented by the mean of the posterior distribution. The two subsurface interfaces are related to: (a) the contact between fine sediments and coarse sediments at ca. 1.0 m depth and (b) between coarse sediments and fine sediments at ca. 7.0 m depth. All inversion results (deterministic and stochastic) are characterized by a low RMS error ($<$3 per cent relative RMS error) indicated also by the data fit curves in Fig. A1.

At borehole LL18, the deterministic and stochastic inversion results of the TEM data reveal a four-layer model for the 6.25 m loop and the 12.5 m loop (Figs A1b and f): (1) a shallow conductive layer ($<$ 10 Ωm) with a thickness of ca. 1.0 m corresponding to silty materials and the unsaturated zone, (2) an intermediate resistive layer ($>$ 30 Ωm) with a thickness of ca. 7.0 m consisting of saturated intermediate sands associated to the shallow aquifer, (3) a confining layer at a depth of ca. 8 m with a conductivity of ca. 15 Ωm due to the clayey silt material and (4) a resistive (ca. 30 Ωm) layer at a depth of (ca. 15 m) corresponding to a deep, sandy aquifer as the electrical resistivity is similar to the shallow aquifer. For the 25.0 m loop (see Fig. A1j) the inversion result reveals a two-layer model that cannot solve the thickness and depth of the shallow aquifer. Yet, we observe the same depth (15 m) to the deep aquifer (ca. 30 Ωm) as obtained from the 12.5 m loop. Due to the inability of the 25.0 m loop to solve for the shallow aquifer, we compare the borehole data only with the TEM inversion results of the 6.25 m and the 12.5 m loops. The first interface between the aquiclude and the aquifer corresponds well to the inversion results for the 6.25 m, but the 12.5 m loop overestimates the thickness of the first interface by ca. 1.0 m. The second interface between the aquifer and the confining silt layer corresponds well to the inversion results for both loops, with a weaker contrast of the electrical conductivity in the 12.5 m loop.

At borehole LL22, the deterministic and stochastic inversion results reveal a three-layer model for the 6.25 m loop and the 12.5 m loops (Figs A1d and h): (1) a shallow conductive layer ($<$ 10 Ωm) associated to silty materials, (2) an intermediate resistive layer (ca. 90 Ωm) consisting of saturated coarse materials from the shallow aquifer and (3) a conductive layer (ca. 20 Ωm) corresponding to the confining layer at a depth of ca. 10 m. The first interface between the aquiclude and the aquifer corresponds well to the inversion results for the 6.25 m, but the 12.5 m loop overestimates the thickness of the first meter by ca. 2.0 m. The second interface at 2.0 m between the aquifer and the confining silt layer corresponds well to the inversion results for both loops. Due to the lack of geological information to support our interpretation, we do not interpret deeper units. Our results reveal that the data collected with the 25.0 m loop lack sensitivity close to the surface to characterise the shallow aquifer similar to borehole LL18 (Fig. A1j), hence we will not further discuss the results of the 25.0 m loop.

Fig. A2 visually shows the information gain at borehole LL22 for the 6.25 m and the 12.5 m loops by comparing the prior data and model spaces to the posterior (after TR rejection) data and model spaces.

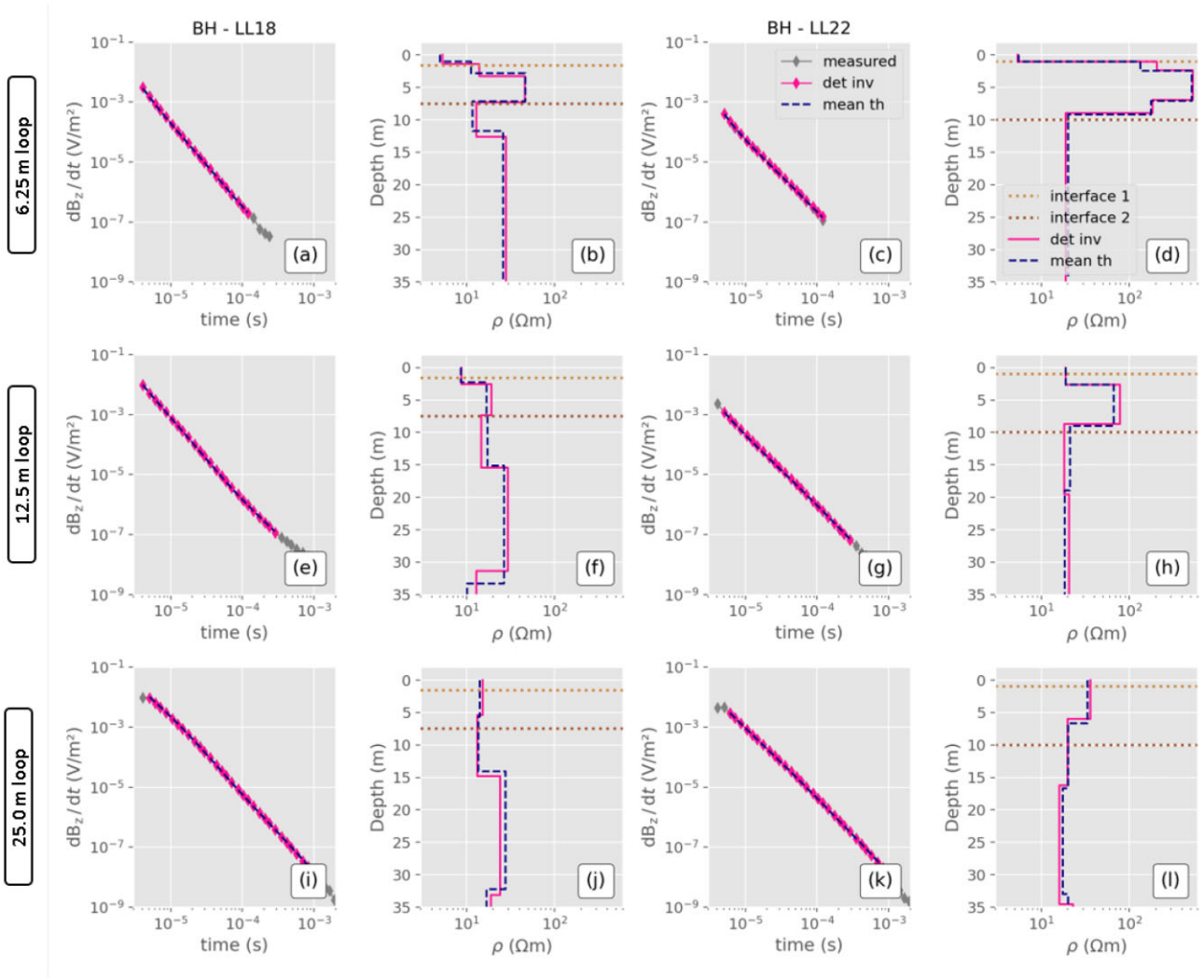

Figure A1. Results from field data measured at boreholes LL18 (a, b, e, f, i and j) and LL22 (c, d, g, h, k and j) for a 6.25 m (a to d), a 12.5 m (e to h) and a 25.0 m square single-loop. The 1-D results depict both the models from deterministic and a stochastic inversion using a threshold to reject models that result in an unrealistic data fit. The horizontal lines depict the contact between fine and coarse sediments at the top (interface one) and coarse and fine sediments at the bottom of the aquifer (interface two).

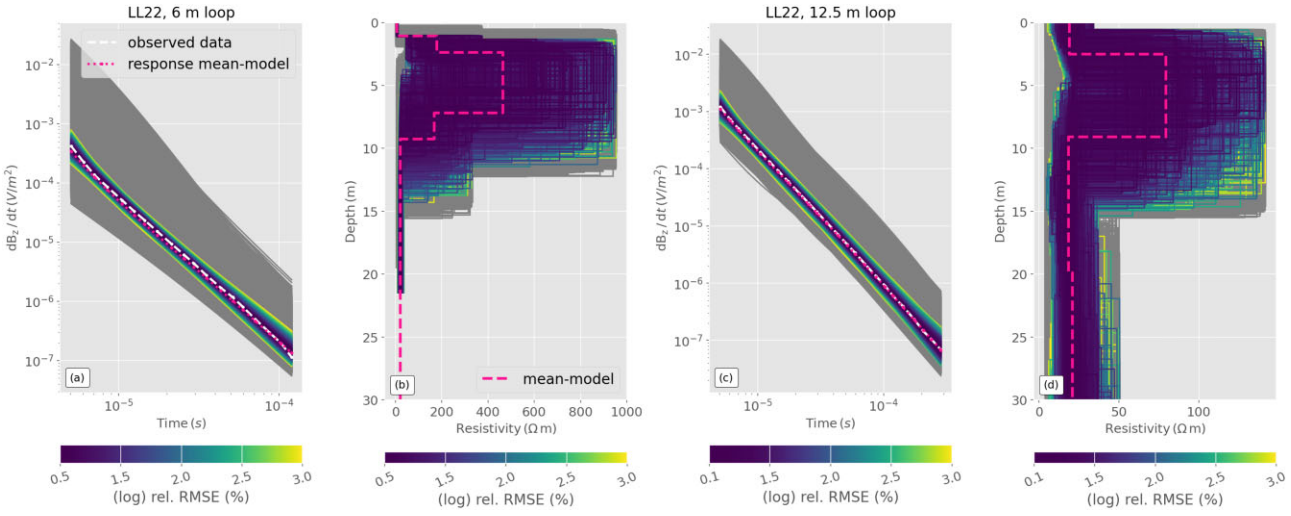

Figure A2. Stochastic inversion results from TEM data measured at borehole LL22 using a 6 m (a, b) and a 12.5 m (c, d) square single loop. Prior data and model spaces are shown in grey in the background, while the coloured lines represent the posterior data and model spaces.

Fig. A3 shows a comparison of the posterior correlation for the individual and the common prior at sounding position L12. The histograms in the main diagonal of Fig. A3 reveal that both prior spaces result in similar posterior distributions that are retrieving the deterministic result with the added value of assessing the uncertainty. In the case of the thickness, both approaches (i.e. individual and common prior) solve for almost the same posterior distributions. The last histogram in the main diagonal of Fig. A3 corresponds to the resistivity of the second layer and reveals that the common prior approach obtains a larger uncertainty than the individual prior.

Fig. A4 shows a comparison of the posterior correlation for the individual and the common prior at sounding position T01. The histograms in the main diagonal of Fig. A4 reveal differences in the posterior distributions obtained from the common prior and the individual prior approach. In the case of the thickness, only the second layer is equally well resolved by both approaches (i.e. individual and common prior). The thickness of the first layer is overestimated by the common prior approach by almost 100 per cent. In the case of the resistivity, the first layer (third histogram of the main diagonal) reveals that the common prior model approach overestimates the resistivity by ca. 50 per cent while the individual prior solves the true model value correctly. This points to an ambiguity between the resistivity and the thickness of the first layer, which cannot be resolved by the common prior space due to the true model value being located at the border of the prior model space. The second and third layer show similar histograms for both approaches, yet the resistivity of the second layer is underestimated in both solutions by ca. 50 per cent. Furthermore, we observe a weak logarithmic correlation between the thickness and resistivity of the first layer, which is likely related to the ambiguity between the first layer thickness and resistivity.

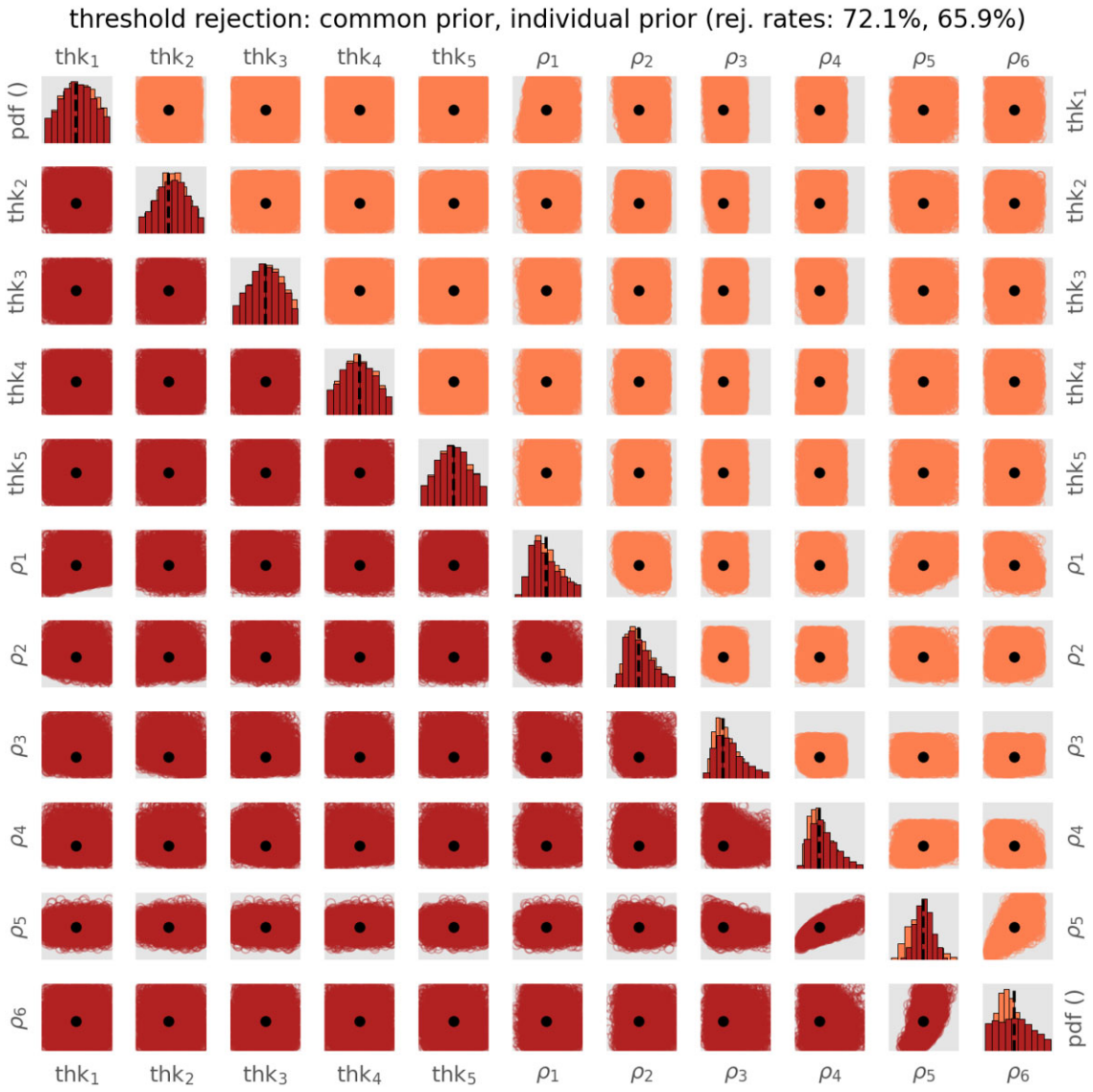

Figure A3. Correlation visualization of the posterior model space for field data results obtained from sounding position L12. The main diagonal shows the probability density for each model parameter and the orange bars correspond to the individual prior results while the red bars correspond to the common prior result. The right triangular entries (light orange circles) show the model parameter correlations for all parameter combinations in model units [thk (m), ρ (Ωm)] corresponding to the individual prior result. The left triangular entries (dark red circles) show the model parameter correlations for all parameter combinations in model units [thk (m), ρ (Ωm)] corresponding to the common prior result. The black dashed line and the black solid dots indicate the values of the deterministic inversion result.

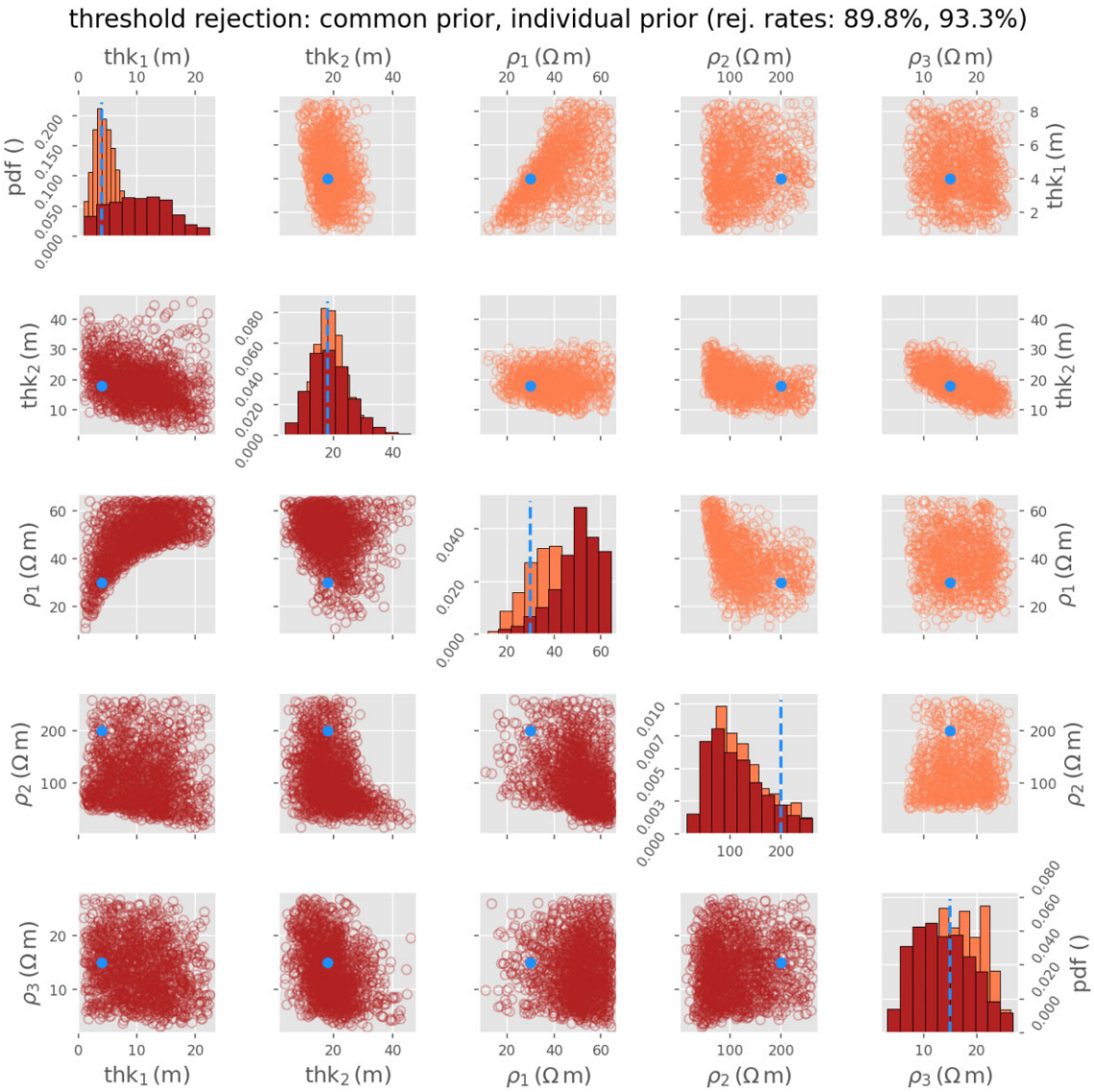

Figure A4. Correlation visualization of the posterior model space for sounding T01. The main diagonal shows the probability density for each model parameter and the orange bars correspond to the individual prior results while the red bars correspond to the common prior result. The right triangular entries (light orange circles) show the model parameter correlations for all parameter combinations in model units [thk (m), ρ (Ωm)] corresponding to the individual prior result. The left triangular entries (dark red circles) show the model parameter correlations for all parameter combinations in model units [thk (m), ρ (Ωm)] corresponding to the common prior result. The blue dashed line and the blue solid dots indicate the values of the true model.